REVIEW

ADVANCED
ENERGY & SUSTAINABILITY
RESEARCH
Open Access

www.advenergysustres.com

Recent Developments in Organic Tandem Solar Cells toward High Efficiency

Fateh Ullah, Chun-Chao Chen,* and Wallace C. H. Choy*

The demands of sustainable energy sources and depletion of conventional energy sources have accelerated the quest for attaining nontoxic and low-cost organic solar cells (OSCs). The intrinsic characteristics of organic semiconductor materials such as light weight, mechanical stability, tailorable bandgaps, and ease of solution processability on a large area with flexible devices provide new dimensions to the device engineers toward sustainable electronic technologies. The past two decades have witnessed an inspiring breakthrough of device efficiency by developing multijunction architectures. The significance of organic tandem solar cells (OTSCs) does not only elevate the efficiencies but also considerably reduces the absorption losses. Herein, the recent developments in OTSCs, starting from designing rules for OTSCs, followed by implementation of the interconnecting layer (ICL) structure, and issues regarding processing, light management, and engaging photoactive materials for constructing OTSCs, are comprehensively described. Finally, the conclusion and outlook for OTSCs are provided.

1. Introduction

Photovoltaics (PV) transform the ubiquitous power of solar energy into electrical energy and are promising contenders to counterbalance the carbon emissions, while delivering an alternative means to address the increasing need of power consumption.[1,2] Numerous PV-based technologies have been developed in the past few decades, e.g., silicon-based (monocrystalline, polycrystalline), gallium arsenide-based, and copper–indium–germanium–selenide-based inorganic solar technologies.[3–6]

However, recent attention has been drawn to organic photovoltaics (OPVs), which are considered to be the promising alternatives in addressing energy insecurity.[7] Organic material foundations (small molecules and polymers) are the auspicious replacements to present inorganic solar cell technologies, due to their distinct properties of low cost, ease of synthesis, mechanical flexibility, large-area printing/coating production, and modest fabrication techniques.[8,9] Scientific communities around the world are investigating various device architectures and engineering new molecular structural designs toward accomplishing competent solar modules.[1] So far, a number of blended material systems including low-bandgap polymers as donor moieties and wide-bandgap small-molecule acceptors or wide-bandgap polymer donors and low-bandgap molecular acceptors have been documented. These vice versa strategies result in enhanced short-circuit current (J_{SC}) and high open-circuit voltages (V_{OC}), whereas morphologies of active organics are cardinal.[10–16] To date, the single-junction bulk-heterojunction (BHJ) OPVs with binary blends have witnessed an astonishing power conversion efficiency (PCE) of 18.22% from solution processing, which is more than ever promising and getting closer to the counter-silicon-based solar cells.[17] However, challenges still exist despite impressive attainable PCEs and demand substantial efforts in producing economically feasible OPV technology, precisely for commercialization.

On this point, various strategies with versatile approaches are under the exploration level of maturity. Among the new device architectures, the tandem concept is advantageous by means of synchronously tackling the voltage losses and effective near-IR absorption of the solar spectrum presented in single-junction OPV devices.[18,19] The organic tandem solar cell (OTSC) architecture involves stacking of two subcell units, one fronting ITO, nominated as the front subcell or bottom subcell, designed for capturing energetic photons in a short wavelength by means of wide-bandgap organics, and one directing the metal electrode denoted as top or rear subcell and assembled for receiving photons with low energies occupying the long wavelength region indulging low-bandgap absorbers.[20–22] In addition, the OTSCs show potential in accomplishing an extensive solar spectrum and resolving associated difficulties concerning the thickness of the active absorbing layers in single junctions due to low carrier mobility.[23] Moreover, thermalization phenomenon can be handled effectively by means of organic semiconductors with

Dr. F. Ullah, Prof. C.-C. Chen
School of Materials Science and Engineering
Shanghai Jiao Tong University
Shanghai 200240, P. R. China
E-mail: c3chen@sjtu.edu.cn

Prof. W. C. H. Choy
Department of Electrical and Electronic Engineering
University of Hong Kong
Pok Fu Lam Road, Hong Kong, P. R. China
E-mail: chchoy@eee.hku.hk

The ORCID identification number(s) for the author(s) of this article can be found under https://doi.org/10.1002/aesr.202000050.

ADVANCED
SCIENCE NEWS
www.advancedsciencenews.com

ADVANCED
ENERGY & SUSTAINABILITY
RESEARCH
Open Access
www.advenergysustres.com

multiple and assorted bandgaps. In this Review, we aim to highlight the recent and most important advancements in the dynamic field of OTSCs with their future perspectives. First, we will address briefly the consideration of single-junction and tandem solar cells. Second, we will confer design rules for efficient material combinations in BHJ OTSCs. Finally, we will review the recent experimental results achieved and documented in well-reputed research journals.

2. Fundamentals of Loss Mechanisms in Single-Junction Solar Cells and Device Architecture of OTSCs

In1961, William Shockley and Hans Queisser derived a mathematical calculation, which assumed the thermodynamically limited PCEs of solar cells caused by direct-bandgap semiconductors used as perfect solar cell absorbers.[24] Following their mathematical predictions, two fundamental phenomena are regarded as the main sources of energy losses in single-junction solar cells (shown in **Figure 1**).

1) Transmission loss: the fraction of energy loss from low-energy photons. Photons carrying low energies with respect to the band edge of semiconductors are optically lost. Limited photo-flux absorption occurs in single-junction solar cells due to the bandgap of absorber material being larger than that of incoming photons. The unused photon energy sequentially gives birth to energy loss. 2) Thermalization loss: the fraction of energy loss from high-energy photons (also known as hot charge carriers). Photons with greater energy than the energy of the bandgap of the semiconductor will thermally relax to the conduction band. The surplus energy above the bandgap of the photoactive material is not used for power conversion and dissipates as heat, giving rise to thermalization loss.

Some theoretical calculations predict that the maximum efficiency of single-junction solar cells is 33.5% with a semiconductor energy bandgap of 1.3–1.4 eV.[24] They theoretically predicted that the tandem architecture consists of two cell configurations, can convert 42%, and triple-cell configuration can utilize 49% of the solar energy under 1 sun irradiation.[25] Theoretically, the calculated efficiency is achievable by enlarging the fundamental parameters of the device simultaneously, including J_{SC}, V_{OC}, and fill factor (FF) via J–V measurements. Introduction of two or more active absorber layers can potentially alleviate these earlier-mentioned fundamental losses. For example, implementation of a wide-bandgap photoactive absorber as the first active layer would minimize thermalization loss featured by hot charge carriers (photons). The following layer should carry low-bandgap semiconducting organics specialized in absorbing photons with low energies. Tandem device architecture effectively reduces these losses produced in single-junction solar cell devices. To construct a tandem device, a couple of organic semiconductors with complementary absorption should be connected in series connection, whereas considering the well-matched optical and electronic nature of these organics is obligatory. Further, an interconnecting layer (ICL) should be inserted between the two stacks containing active organic materials, whereas the ICL cardinally delivers a platform for charge recombination by means of receiving charges from adjacent absorbing layers. The ICL involves a double-layer architecture, engineered of a p-type hole-transporting layer (HTL) and an n-type electron-transporting layer (ETL), both functioning as a charge recombination layer with appropriate Ohmic contact guaranteeing fast charge recombination and evading voltage losses.

Finally, tandem devices forming a series connection should add up the voltages of the subcells. Generally, the V_{OC} of OTSCs should be the sum-up value of the individual subcell devices, whereas the J_{SC} of OTSCs is limited by the least J_{SC} in all subcell units. To minimize the thermalization loss concerning individual devices in a tandem, the individual device energy loss, E_{loss} ($E_{loss} = E_g - eV_{OC}$, where E_g represents the active layer optical bandgap, e denotes the elementary charge, and V_{OC} represents the open-circuit voltage), in a tandem should be minimal guaranteeing a higher V_{OC}.[26,27] Nevertheless, attention should be delivered to a couple of challenges. First, the condition of incident light involving single-junction architectures and corresponding subcell units used for constructing OTSC devices might be quite different. In other words, the subcells of
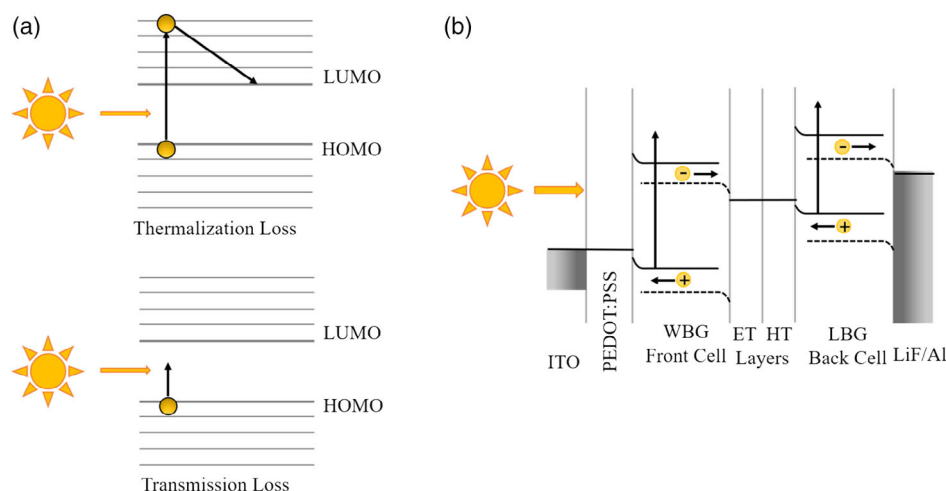

Figure 1. a) Fundamental of loss mechanism. b) Energy-level diagram of a polymer tandem solar cell.

**ADVANCED
SCIENCE NEWS**

www.advancedsciencenews.com

**ADVANCED
ENERGY & SUSTAINABILITY
RESEARCH**
Open Access

www.advenergysustres.com

OTSCs might face low-intensity conditions, which can possibly impact the V_{OC} of each subunit in a tandem. Second, the unfavorable energy-level alignments flanking ICL and active layer may contribute to electrical loss ultimately influencing V_{OC}.[28,29] Accordingly, minimizing the offset between the band energy and carrier recombination at the junction of transporting layer/active layer interfaces can be useful in facilitating the charge transmission as well as addressing the V_{OC} loss in OTSCs.[30] Similarly, the introduction of efficient transporting and recombination materials in OTSCs could be a competent approach toward minimizing V_{OC} loss.[31–33] Moreover, a proper design of energy levels of organics will encourage V_{OC} as well. In this case, the difference between the highest occupied molecular orbitals (HOMO) of the donating materials and lowest unoccupied molecular orbital (LUMO) of the acceptor is proportional to V_{OC}. So, increasing the LUMO of acceptor and deepening HOMO of the donor could be a useful strategy for enhancing V_{OC}.[26] Based on the discussion earlier, the tandem architectures have the tendency to overwhelm the fundamental limitation of single junctions. The serially connected tandem junctions with complementary absorbers and careful architecture design to minimize V_{OC} loss can eventually deliver maximized efficiency performance.[29]

3. Design Rules of Materials for OTSCs

A suitable ICL has to fulfill the subsequent considerations: a) transparency of the ICL (even at highly thick ICL depositions) is cardinal in terms of minimizing light absorption in the visible and near-IR region; b) Ohmic contact between subcells and intermediate layers is needed to minimize the energy loss for inflowing charges to the intermediate layers from photoactive layers; c) the ICL should permit efficient charge recombination with minimal electrical resistance and prevent the subcells from receiving unwanted electrons and holes due to incomplete recombination; d) during subsequent fabrication, the ICL's solvent orthogonality and physical robustness are essential, shielding the underlying deposited layers from being dissolved or damaged; and e) in addition, facile technologies with least investment (with the potential of yielding elevated processing throughputs) should be engaged when depositing ICLs.

Designing and engineering photoactive materials for each subcell (with different bandgaps and complementary selective absorption) in inspiringly efficient OTSCs is vital. Some fundamental attention is granted to the following aspects for efficient OTSCs: a) scheming affordable photoactive absorbers (for polymers and small molecules) from abundant and economical starting molecular entities that require fewer synthetic steps with outstanding and reproducible scale-up production; b) engineering organics (donors and acceptors) in different subcells toward complementary photo-flux absorption, matched photocurrent output, and superior charge carrier mobilities (even under thick-film conditions); and c) enhancing device stability via stable material designing and encapsulation technologies.

4. ICL Materials

In OTSCs, the subcells are connected together by ICL structures. The selection of ICL is cardinal in gaining the optimal performance for OTSCs. Requisitely, ICL should stack the subcells electrically (establishing an identical Ohmic behavior, eventually eliminating V_{OC} losses) and optically (uniform high transparency permitting photo-flux to be absorbed by both subcells). ICL should also provide a potent platform for the deposition of top subcells and prevent dissolving the bottom subcell via solvent penetration.[34] The ICLs generally involve a double-layer architecture engineered of p-type and n-type materials, extracting electrons and holes selectively, both functioning as charge recombination layers. Mostly, the ICL is the combination of polymeric material and metal oxide nanoparticles, e.g., poly(3,4-ethylenedioxythiophene): polystyrene sulfonate (PEDOT:PSS) working as HTL and zinc oxide (ZnO) nanoparticles as ETL. In addition, a variety of other emerging materials such as evaporated molybdenum oxide introduced as HTLs, coated by a thin discontinuous silver layer, and poly[(9,9-bis(3′-(N,N-dimethylamino)propyl)-2,7-fluorene)-alt-2,7-(9,9-dioctylfluorene)] (PFN) functioning as ETL are documented. Moreover, new materials have been introduced by the scientific community, e.g., conjugated polyelectrolytes (CgPEs) and pH-neutral semiconducting polymers (SCPs) with self-doping characteristics. Both CgPEs and SCPs can produce dipole moments with the ease of tuning interfacial work function by their anionic and cationic functionalities. For the same reason, the thickness of the ICL has to be critically thin to maintain the dipole moment arrangement.

4.1. Organic Semiconducting Polyelectrolytes Functioning as ICL

Zhou et al. documented two novel CgPEs, PCPDT-BTSO$_3$K (CPE-K) and phenyl-based PCPDTPhSO$_3$Na (CPEPh-Na) (shown in **Figure 2**a).[35] Attributed to the alkylated ionic side functionalities, a thin layer (10–15 nm) of these HTLs effactually upsurged the interfacial work function homogenously to 5.2 and 5.15 eV for CPEPh-Na and CPE-K, respectively, presenting a much deeper work function than that of the n-PEDOT:PSS HTL (4.75 eV). The optimized tandem devices utilizing a ZnO nanoparticle layer coated with CPEPh-Na as ICL presented an enhancement of 25% to that of single cells and delivered a PCE up to 11.3%. Cui et al. implemented a chemically similar ICL based on ZnO and a pH-neutral self-doped p-type CgPE PCP-Na; the optimized thickness of ICL realized an efficiency over 13% under an illumination of 0.02–1 Sun in tandem with state-of-the-art photoactive materials.[36] Lee et al. successfully reported a new polymer abbreviated as p-PFP-O, synthesized via oxidative doping of PFP-O by means of ammonium persulfate potentially reversing its electronic properties.[37] The ultrathin layer of p-PFP-O ($\approx$2 nm) successfully increases the work function of the electrode by forming an interfacial dipole, facilitating hole extraction from the photoactive layer. The tandem device based on ZnO/PEDOT-SO$_3$Na/p-PFP-O as an ICL, having low-work-function pH-neutral PEDOT-SO$_3$Na, can avoid the loss of V_{OC} and eventually generate a PCE of 10.2% with extended stability. Zhang et al. presented an ICL design using PF3N-2TNDI as a potent CgPE for n-side channel, PEDOT:PSS for the p-side channel, and an ultrathin silver layer deposited in between for improving recombination characteristics of the subcells.[38] The afresh-designed ICL efficaciously protected
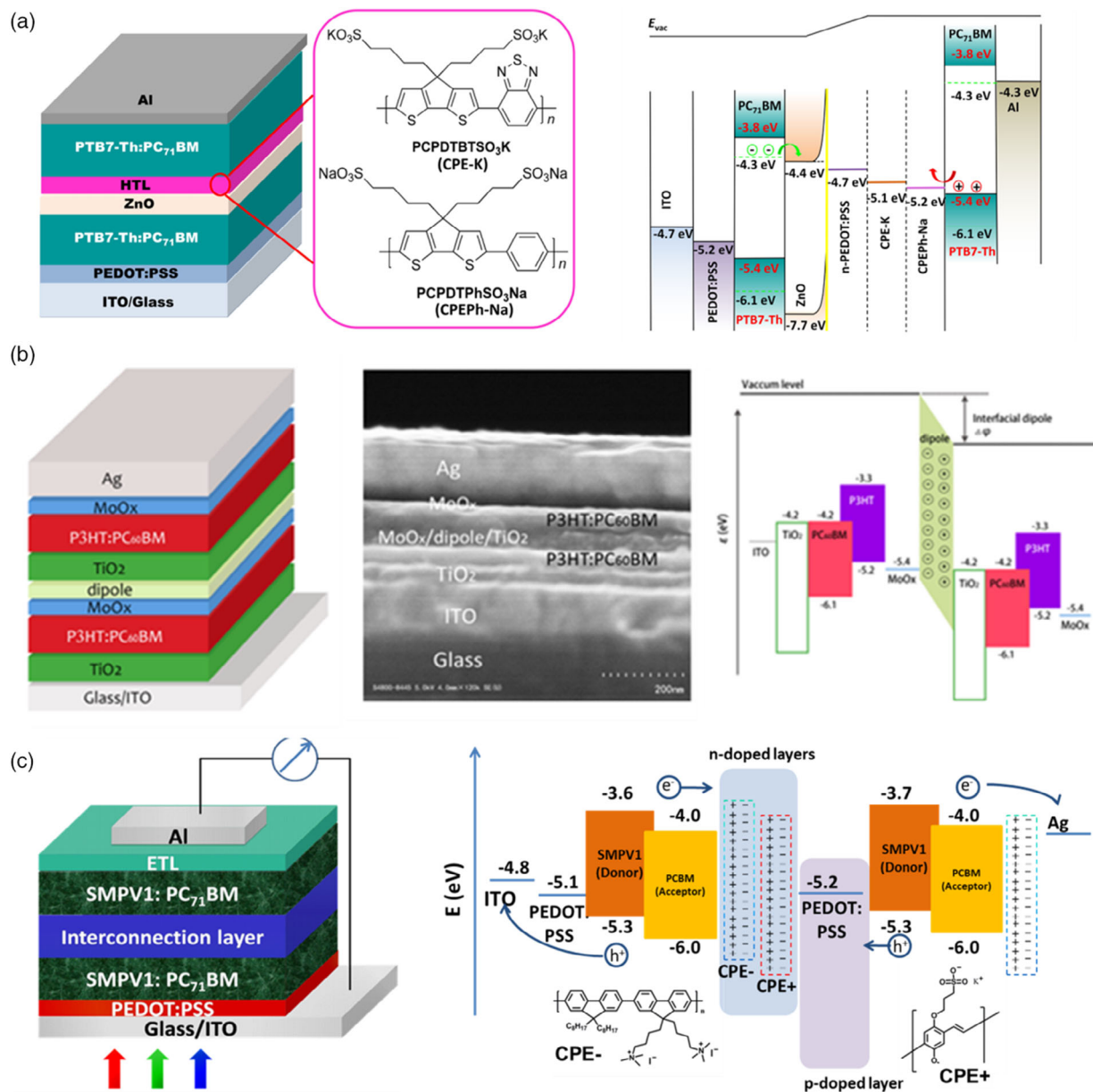
Figure 2. Homo-tandem solar cells. a) Device structure of tandem with ZnO/PEDOT:PSS/CPE and its used chemical units and band diagrams. Reproduced with permission.[35] Copyright 2015, Wiley-VCH GmbH. b) Device structure of tandem cells with MoOₓ/dipole/TiO₂ along with cross-section results of transmission electron microscopy and energy diagrams. Reproduced with permission.[44] Copyright 2018, Wiley-VCH GmbH. c) Device structure of the tandem with the CPEs/PEDOT:PSS structures and energy diagram as well. Reproduced with permission.[45] Copyright 2013, Springer Nature.

the bottom subcell from solvent erosion and potentially reduced the work function of silver from 4.5 to 4.1 eV. The OTSC device using this newly engineered ICL accomplished a high PCE of 11.35%. The implementation of this ICL in fabricating flexible OTSCs provided a PCE of 10%. The same research group blended PF3N-2TNDI with polyethyleneimine (PEI).[39] Bearing numerous amine functionalities, PEI could largely reduce the work function of PEDOT:PSS without sacrificing the charge transport ability.[40] An optimal mixture ETL:PEI (3:2)/PEDOT received a high-performing OTSC and eliminated the need of an extra silver layer in between ETL and PEDOT:PSS. The

OTSC devices afforded a high PCE of 12.6% with ICL thickness of 60 nm and even approached 11.3% with increased ICL thickness of 140 nm, demonstrating the material ability toward large modules. Furthermore, by printing a homojunction all-polymer OTSCs, they fruitfully obtained a high PCE of over 11% with thermal stability (90%) at 80 °C for 1000 h.[41] Zuo et al. individually reported OTSCs by adopting PFN.[42] Their versatile ICL containing evaporated molybdenum oxide (MoO₃), followed by an ultrathin layer of silver with PFN on top, achieved a high PCE of around 11% with an extraordinary summed external quantum efficiency (EQE) peak value beyond 90%. Following

**ADVANCED
SCIENCE NEWS**

www.advancedsciencenews.com

**ADVANCED
ENERGY & SUSTAINABILITY
RESEARCH**
Open Access

www.advenergysustres.com

the same approach, Martínez-Otero et al. obtained a particularly high FF of 0.76, regardless of the entire thickness of ICL being below 20 nm.[43] Both research groups successfully documented the altering of MoO_3/Ag surface by means of PFN that can potentially reduce its work function, while preserving high optical transparency and robustness of the ICL as well. Lu et al. demonstrated a novel ICL comprising metal oxide/dipole layer/ metal oxide with the dipole layer (n-type CgPEs) processed from their respective solutions (shown in Figure 2b).[44] The water-/ alcohol-soluble amino-functionalized polymer PF6N25Py was deposited on top of molybdenum bronze layer. The work function of MoO_3 can be effectively tuned, enhancing energy-level alignment with a subsequent film of titanium dioxide (TiO_2) nanoparticles. The fabrication of homo-OTSC devices utilizing the current ICL yielded in almost no V_{OC} loss in comparison with each subcell alone and retained a comparable FF, referring single-junction devices with elevated performance. One of the earlier works presented by Liu and coworkers using two CPEs with anionic and cationic groups showed that they can self-assemble to form a robust ICL layer without thermal annealing. Small-molecule-based tandem solar cells using this ICL design and identical absorber in two subcells delivered 10% PCE (shown in Figure 2c).[45]

4.2. Metal Oxides Combined with PEDOT:PSS-Based Material for ICL

Metal oxide semiconductors are a promising class of charge extraction interlayer materials, generally for electronics and specifically for OPV devices. The deposition of metal oxides in OPV is generally done from either nanoparticle suspensions, or from a solution of metal–organic precursors converting them to subsequent metal oxides, or via thermal evaporation using high vacuum. Introduction of all-oxide (metal oxide) ICLs continuously involves the application of thin metal clusters, benefitting from their conductivity and stability as well. Individual works by Chou et al. and Zhao et al. successfully documented the incorporation of metal oxides to the inverted tandem architectures.[46,47] Bag and coworkers provided a chemically robust ICL for OTSCs, comprising a thermally evaporated chromium (Cr) and molybdenum trioxide (MoO_3) bilayer, revealing high transparency above 375 nm. Eventually, the fabricated monolithic OTSCs showed moderate PCEs.[48] A limited number of metal oxides contributed to the ICL list for OTSCs conceivably on account of guaranteeing the protection of active material of bottom subcells against the solution fabrication processing of the top subcell active material.[38] A solitary example was provided by Becker et al., utilizing an all-oxide ICL in fabricating inverted (n–i–p) polymer OTSCs.[49] The novel recombination layer comprised thermally evaporated molybdenum oxide as HTL with high work function (WF) and low-WF tin oxide (SnO_x) acting as ETL, stacked together via atomic layer deposition. A large intrinsic interface dipole formation occurred at the interface of HTL/ ETL, possibly inferring an ideal alignment of the conduction band of MoO_x and SnO_x. Such an ICL is beneficial in reducing voltage losses and UV light soaking. Recently, Rasi et al. fabricated OTSCs with tin oxide (SnO_2) functioning as ETL via solution processing.[50] Fabrication was accompanied by chemically

compatible PEDOT:PSS as HTL and demonstrated efficient OTSCs with both conventional (p–i–n) and inverted (n–i–p) architectures. SnO_2 provided a ground with the possibility of eliminating low-work-function pH-neutral PEDOT:PSS usually involved in voltage losses. In addition, SnO_2 potentially resisted the acidic nature of commercially formulated PEDOT:PSS while washing out ZnO layer. Furthermore, the combination of SnO_2/ PEDOT:PSS as ICL could be utilized in both conventional and inverted architectures deprived of supplementary coatings. Silva and coworkers utilized a robust ICL composed of a mixture of PEDOT:PSS as HTL in combination with lithium-doped zinc oxide (LZO) as ETL. The fabricated OTSCs utilizing this ICL revealed high V_{OC}.[51] Congruently, Mitul et al. used aluminum-doped ZnO (AZO) via solution processing, achieving low-temperature-processed and chemically robust PEDOT:PSS/ AZO/PEIE-based ICL.[52] Homo-OTSCs were fabricated with active material based on P3HT:PCBM, whereas AZO was thermally annealed using precursors. Their device architecture fabricated by this ICL not only sustained elevated temperature but also revealed high V_{OC}.

Du et al. provided a solution to the interfacial losses taking place in OTSCs using PEDOT:PSS as HTL.[53] The author reported that fabricating PEDOT:PSS on top of the active material layer protonates the nitrogen atom in the polymer backbone. This protonated film possibly suppressed the hole transporting properties of PEDOT:PSS. They introduced facile solution mixing of MoO_x nanoparticles and PEDOT:PSS, which effectively dominated the interfacial losses, by means of reducing interface protonation and providing improved energy-level alignment with smooth and dense layer formation. Using this hybrid ICL based on PEDOT:PSS:MoO_3/ZnO/PEI, enhanced performance in comparison with the controlled OTSC devices carrying only PEDOT:PSS or MoO_3 is demonstrated. You and coworkers designed a homo-tandem solar cell using two identical near-IR polymeric absorbers to enhance the overall absorption of the device. In their architecture design, MoO3/ PEDOT:PSS/ZnO was utilized as ICL. Thermal-evaporated MoO_3 can decrease the interfacial work function between PEDOT:PSS and the HOMO of the bottom subcell (shown in **Figure 3**a).[54] Similarly, Torabi et al. used a homo-tandem device architecture to achieve high V_{OC} with a moderate FF in comparison with the reference devices.[55] They synthesized Ag/PEDOT:PSS-based nanocomposite functioning as HTLs within the ICL, whereas sol–gel TiO_2 worked as ETL. Dispersion of modified PEDOT:PSS was used as the medium to obtain Ag nanoparticles directly from the reduction of its silver nitrate precursor with sodium borohydride, eliminating the necessity of any stabilizer. Recently, Raïssi et al. used PEDOT: PSS/Ag nanowires/ZnO nanoparticles as an ICL in fabricating OTSCs.[56] They suggested that the ICL could provide optimal carrier transportation and an efficient recombination center for the subcells. For constructing triple-junction OTSCs, Chen et al. implemented an ICL composed of WO_3/PEDOT:PSS/ ZnO.[57] Here, WO_3 nanoparticles can reduce the energy barrier between PEDOT:PSS and bottom subcell. The thin layer of WO_3 was deposited from alcohol suspension (shown in Figure 3b). Finally, the current state-of-art OTSCs with 17.3% efficiency adopted the modified PEDOT:PSS/ZnO for ICL design (shown in Figure 3c).[58]
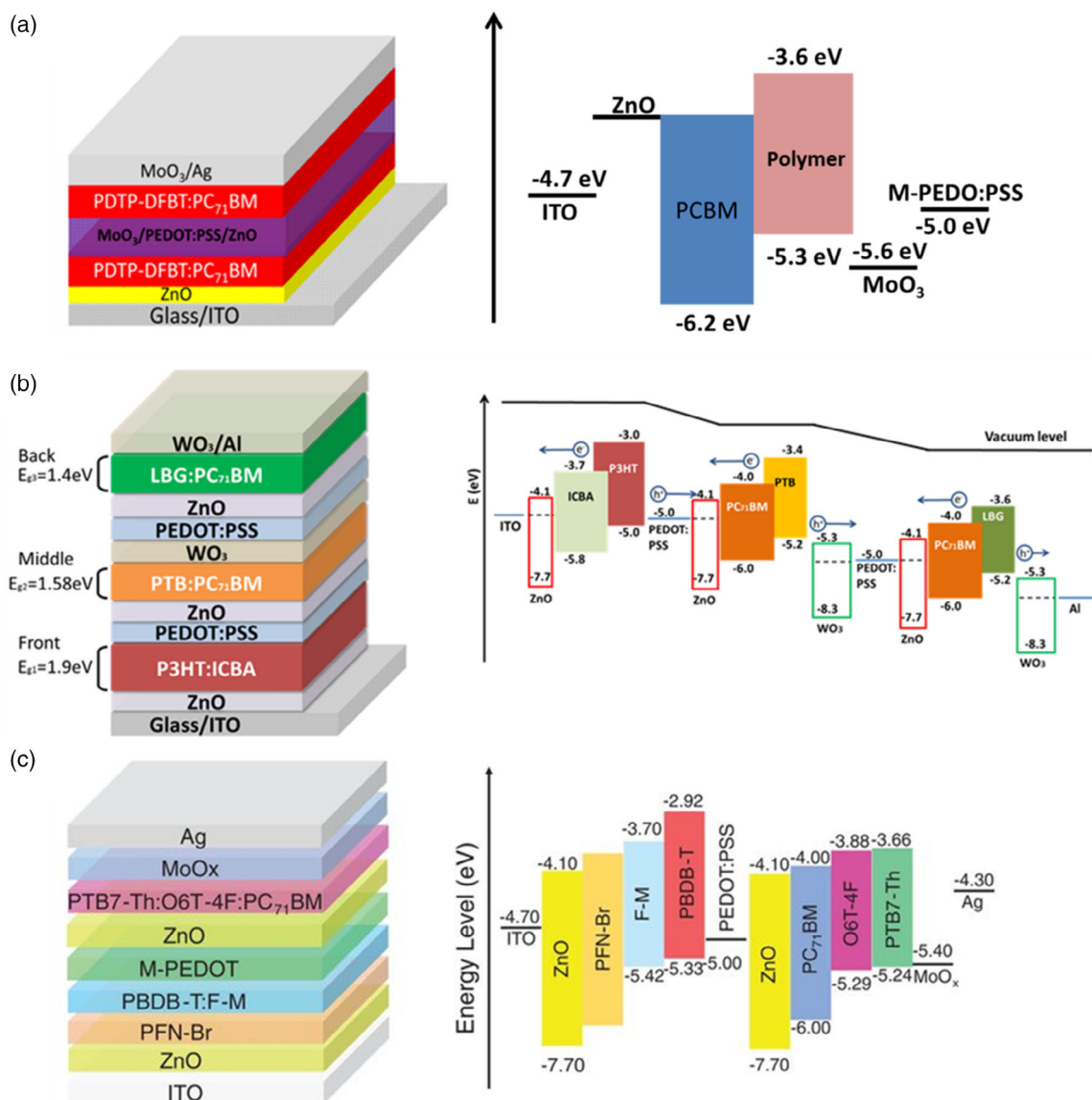
Figure 3. a) Tandem device structure and energy levels of ICL design: MoO$_3$/PEDOT:PSS/ZnO. Reproduced with permission.[54] Copyright 2013, Wiley-VCH GmbH. b) Layer stacks of the triple-junction tandem solar cell in the inverted architecture and energy levels for ICL design: WO$_3$/PEDOT:PSS/ZnO. Reproduced with permission.[57] Copyright 2014, Wiley-VCH GmbH. c) Tandem device structure and energy-level representation of ICL design: PEDOT:PSS/ZnO. Reproduced with permission.[58] Copyright 2018, The American Association for the Advancement of Science (AAAS).

4.3. Metal–Organic-Based Hybrid Material for ICL

Recently, Lu et al. emerged with the new idea of using metal–organic molecular chelates in OTSCs as ICL.[59] Their work involved zirconium acetylacetonate (Zr-acac) insertion in formulating new ICL (PEDOT:PSS/Zr-acac/PF6N25Py), which considerably reduced the work function of PEDOT:PSS from 5.0 to 3.49 eV and led to V_{OC} loss as well (**Figure 4**a). Later, Chang et al. elaborated the potentials of utilizing Zr-acac in developing ICL MoO$_3$/PEDOT:PSS/Zr-acac.[60] They revealed the electrical and optical characteristics of Zr-acac and their advantages of simplifying solution processability and escaping any additional thermal annealing. Tan and coworkers documented another

metal chelate, based on titanium (diisopropoxide) bis(2,4-pentanedionate) (TIPD), for modification of electrode and ICL as well (Figure 4b).[61] They fabricated TIPD from isopropanol over an evaporated layer of MoO$_3$/Ag functioning as ICL, following by post-treatment with 150 °C to achieve an optimal performance for OTSCs. They concluded that using MoO$_3$/Ag/TIPD as ICL, high transparency with minimized voltage losses was achieved. Earlier research documentation has revealed that pH-neutral PEDOT:PSS usually does not accomplish the criteria of matching the deep HOMO energy level of photoactive polymeric material, governing V_{OC} loss.[62] Continuing with metal complexes, Lu et al. developed a switchable ICL for both conventional and inverted tandem architectures.[63] The ICL included a
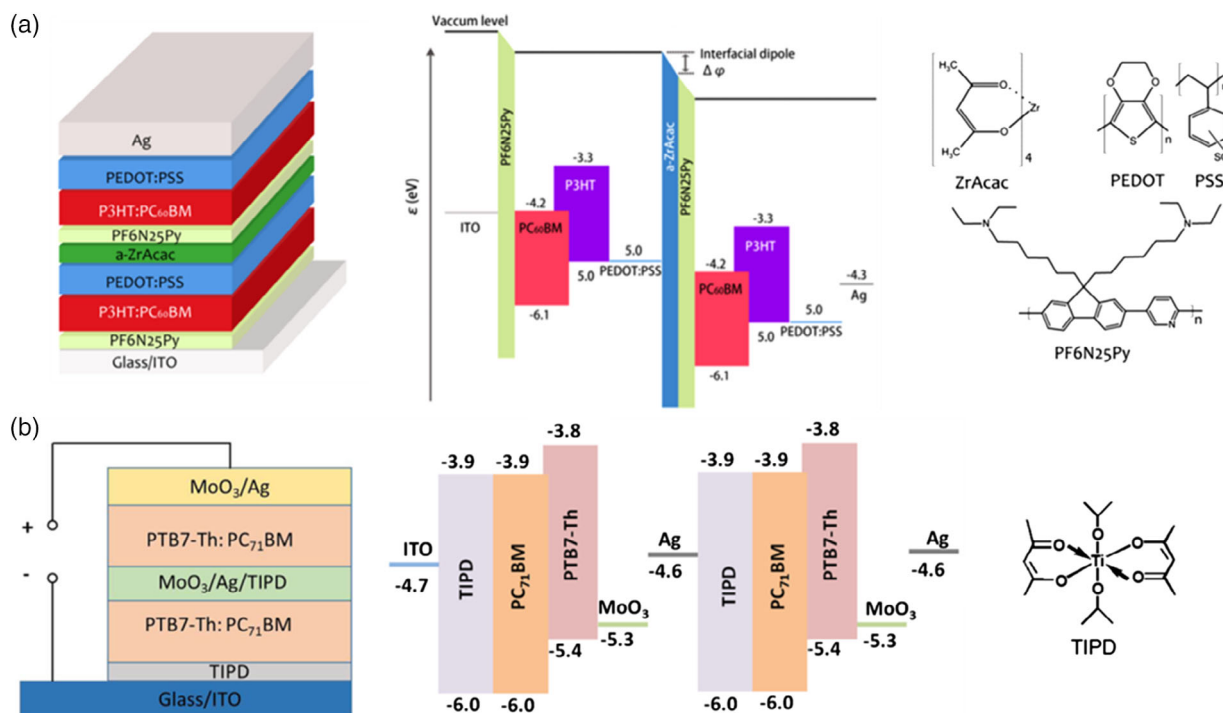
Figure 4. a) Tandem device structure, energy levels, and chemical structure of ICL design: PEDOT:PSS/ZrAcac/PF6N25Py. Reproduced with permission.[59] Copyright 2016, Elsevier. b) Tandem device structure, energy levels, and chemical structure of ICL design: MoO$_3$/Ag/TIPD. Reproduced with permission.[61] Copyright 2018, CAS, Shanghai & Wiley-VCH GmbH.

pH-neutral PEDOT:PSS serving as recombination layer along with phosphomolybdic acid hydrate (PMA) for extraction of charges and ZnO nanoparticles solely functioning as ETL. The introduction of PMA to pH-neutral PEDOT:PSS facilitated the energy-level alignment with its corresponding polymer material with a deep HOMO energy level, avoiding V_{OC} loss. The authors revealed a potential recovery in V_{OC} loss using the ICL constructed of PMA/PEDOT:PSS/ZnO for inverted OTSCs. Vasilopoulou et al. implemented annealing-free crystalline metal oxides processed from methanol forming ICL for tandem architectures.[64] The bottom subcell contained P3HT:ICBA as an active material, whereas top subcell utilized PTB7:PC$_{70}$BM combination. The active material of the bottom subcell was covered by a layer of polyoxometalate (POM) as HTL, subsequently followed by the introduction of ZnO nanoparticles utilized as ETL. Following the previously selected POM, the authors selected $(NH_4)_6P_2Mo_{18}O_{62}$ with highly attractive electronic characteristics, i.e., work function and very deep HOMO and LUMO energy levels of 8.2 and 5.6 eV, respectively. The authors anticipated that the presence of such deep LUMO energy levels of POM can align the HOMO energy level of the donating polymer. Generally, such deep LUMO energy levels play a cardinal role in the recombination process as p-doping agents within ICL, hence beneficial for device performance. The results obtained after tuning the electronic characteristics of polymeric donors revealed almost loss-free V_{OC}. All the device data including J_{SC} and FF supported the performance of the OTSCs device, except the summed EQE of the subcells, appearing to be 150% and contradicting to support the device operational value.

4.4. Allotropic-Carbon-/Carbon-Quantum-Dots-Based Material as an ICL

The marvelous nature, diverse characteristics, and flexible features (both physical and chemical) made carbon extraordinarily valuable.[65–67] In addition, the ecofriendly, simple, and low-cost processing of carbon-based material is a plus.[68] Chang et al. presented a thermally cross-linkable acid-based fullerene derivative C-PCBN$_3$, n-doped with tetrabutylammonium iodide (TBAI), serving as ETL ahead of PEDOT:PSS as HTL.[69] Moreover, a low temperature of 140 °C was used for cross linking, potent in terms of fabricating the ETL on compatible flexible substrates, i.e., polyethylene naphthalate. In addition, for TBAI, its judicious electrical conductivity, decent stability (both ambient and chemical), and work function tenability all contributed to the impressive PCE on flexible substrate in comparison with the counter on glass substrate. The ETL of TBAI is thickness sensitive with an optimal thickness of 10 nm. Single-walled carbon nanotubes (SWCNTs) entrenched by polymeric environment (both covalently and noncovalently by organic or aqueous media) appeared to be promising candidates, due to their transparency, high conductance in thin films (both electrical and thermal), outstanding stabilities (both chemically and mechanically), high aspect ratios with nanoscale diameter, and appropriate electronic structures.[70–72] Raïssi et al. displayed an ICL constructed of single walled nanotube with metallo-phthalocyanine complex (TSCuPc) as an ETL on the top of PEDOT:PSS, ensuring HTL features.[73] Kang et al. documented an another allotropic form of carbon, carbon quantum dots (CQDs) mixed with an
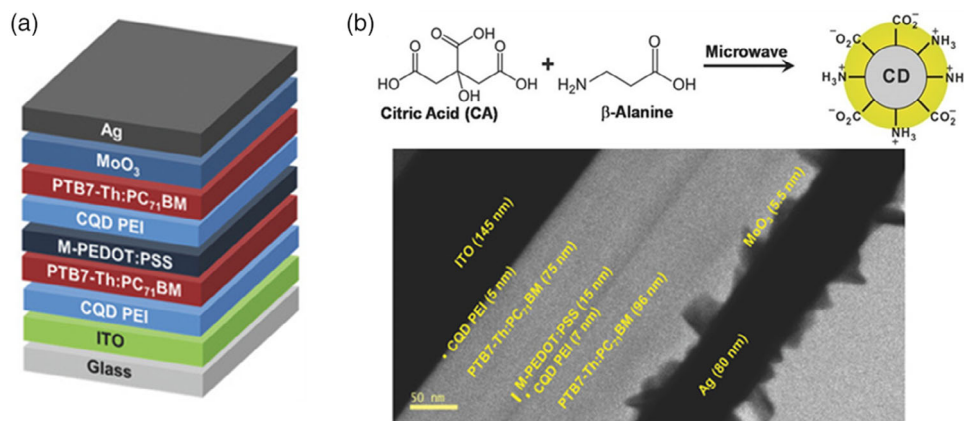
**ADVANCED
SCIENCE NEWS**
www.advancedsciencenews.com

**ADVANCED
ENERGY & SUSTAINABILITY
RESEARCH**
Open Access
www.advenergysustres.com

Figure 5. a) Tandem device structure of ICL design: M-PEDOT:PSS/CQD/PEI. b) Scanning electron microscopy cross-section image of ICL and synthesis of CQD. Reproduced with permission.[74] Copyright 2018, Wiley-VCH GmbH.

intermediate PEI (see **Figure 5**a,b).[74] The CQDs were synthesized by pyrolysis from its starting material citric acid and β-alanine by microwave, which resulted in particles' nanometer size (≈3 nm). The ICL consisted of PEDOT:PSS as HTL and a thin layer of the CQDs/PEIE nanocomposite on top of it. The fabrication of homo-OTSCs revealed high efficiencies with the insertion of CQDs/PEI layers, which potentially provided better electron extraction connected via series connection in tandem architectures. Besides CQDs, the graphene quantum dots (GQDs) exhibit highly attractive features, such as narrow size distribution, elevated mobility, and bandgap tenability, which also suggest their potential as HTLs for solar panels. The only negative factor in GQDs is its poor film formation on top of active material. Thus, GQDs can only be utilized in conventional devices.[75,76] Doping of material can potentially alter the characteristic features of GQDs.[77,78] Ho et al. proposed an ICL containing nitrogen-doped GQDs (N-GQDs) with PEI to fabricate inverted OTDCs.[79] N-GQDs were synthesized in a Teflon-lined autoclave using a mixture of citric acid and ammonia at an elevated temperature; finally, the pH was adjusted by sodium hydroxide solution at ambient temperature. The authors further reported that an increase in shunt resistance was observed in devices carrying N-GQDs ($8.68\,\Omega\,cm^2$) in comparison with PEDOT:PSS ($4.80\,\Omega\,cm^2$), although having same series resistance and J_{SC}, suggesting balanced charge collection. In addition, the N-GQDs possessed outstanding hydrophilicity and stability against aqueous media. Moreover, N-GQDs formed a dipole with PEI, in which electron-deficient O—C—O functionality provided a high work function.

5. Processing Issue in OTSCs

One of the major challenges in commercialization of the future OPV/OTSC technology is the fabrication and stacking of two subcells without washing out the lower layers during the manufacturing processes. To do so, the choice of the solvent for each layer has to satisfy the deposition of the specific material layer and avoid damaging the underneath layer structure. First, solvents for the bottom subcell are nonpolar organic solvents,

such as chlorobenzene and dichlorobenzene, without many limitations. Second, solvents for ICL are selected from polar solvents, such as IPA, water, and ethanol, to avoid redissolving organic bottom subcells. For example, PEDOT:PSS is mainly deposited from water dispersion with high surface energy, whereas most photoactive materials possess hydrophobic nature. So, the involvement of surfactants or IPA is often needed to reduce the surface energy and allow uniform coating. Finally, solvents with low boiling points, such as chloroform and methylene chloride, have been already used in top subcell processing to avoid damaging the bottom subcell.[80] If low-boiling-point solvents are not suitable for processing top subcells, then a robust and solvent-resistant ICL is required to physically protect the underlying bottom subcells from any damage and destruction throughout a wide range of solvents and additives used for top subcells. To ensure the robustness of PEDOT:PSS layer, thermal annealing above 120 °C is often required. Sometimes, cross linking of ICL is favorable to resist certain corrosive and high-boiling-point solvents used for top subcells.[31] Furthermore, the current OTSCs architecture implements two or more subcells stacked together and each subcell comprises a multilayer of photoactive components, interfacial material, and ICL functioning as the recombination layer.[35,54,57,81,82] Such complex tandem architectures significantly increase difficulties in printing procedures and eventually intensify the cost of production for commercialization.[83,84] In this section, we briefly summarize the recent reports concerning the processing of OTSCs.

Wei et al. implemented a novel concept of self-organized buffer layer formation in single-junction OPVs.[85] They introduced the photoactive components and materials forming an ICL from an identical solution. Their strategy revealed that an insertion of fullerene material, F-PCBM, from the same solution could assist the spontaneous migration of materials to the surface due to different surface energies and form a thin buffer layer on the top surface. From 2015, their strategy of self-organization was followed by Lee's research group to fabricate tandem architectures.[37,86,87] Their solution preparation included a simple mixing of polyelectrolyte (PEI) with photoactive material for the blend preparation. PEI with diverse surface energies could spontaneously separate from the photoactive blend during the
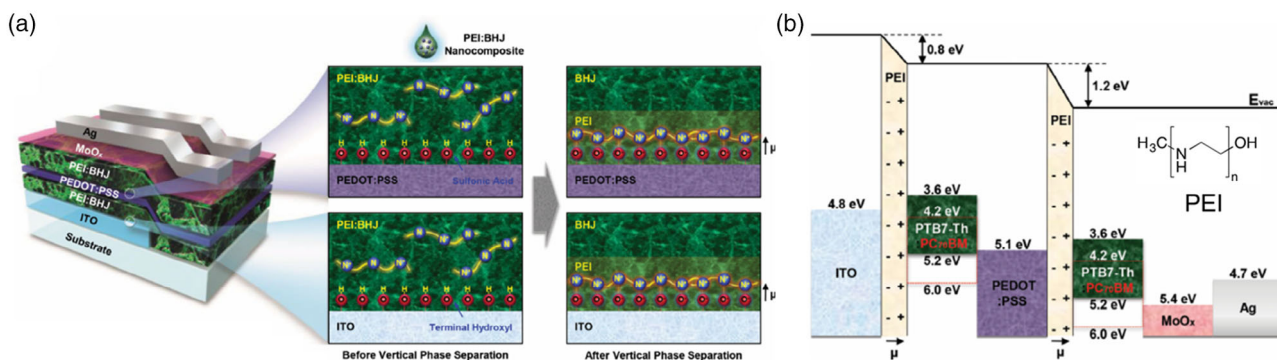
Figure 6. a) Tandem polymer architectures fabricated via BHJ:PEI nanocomposite solutions. b) Energy-level illustration of the tandem solar cells. Reproduced with permission.[86] Copyright 2014, Wiley-VCH GmbH.

fabrication process (shown in **Figure 6**). By the same technique, they fabricated an inverted tandem device using an ICL comprising PEDO:PSS/PEI for two PTB7-Th:PC$_{70}$BM BHJs.[86,87] They confirmed their scientific understanding of PEI dispersion by time-of-flight secondary-ion mass spectrometry measurements. The confinement of PEI was observed on both top and bottom subcells vertically following the stack. Recently, Chen et al. developed an improved PEDOT:PSS/ZnO as ICL for homo-tandem devices.[88] The recombination layer was based on wet PEDOT:PSS, followed by a processed layer of diethyl-Zn precursor-based ZnO on the top, resulting in an ICL. According to the authors, the ZnO layer formation required mild heating. Thus, the moisture that existed in PEDOT:PSS film reacted chemically with the precursor based on diethyl ether (highly sensitive to moisture). As a result, moisture was taken away from PEDOT:PSS by the diethyl-Zn precursor to turn diethyl-Zn into ZnO. The then-prepared OTSC devices revealed an elevated V_{OC} of 2.16 V with moderate PCE.

Establishing an inverted tandem architecture is challenging due to the poor reproducibility of the smooth PEDOT:PSS layer formation. PEDOT:PSS is mainly deposited from water dispersion with high surface energy, whereas most of the photoactive materials are of hydrophobic nature. So, the involvement of surfactants (an insulating material) is desired to lower the surface energy. However, the presence of the surfactant also restricts the characteristic features of PEDOT:PSS, e.g., conductivity and work function. In addition, PEDOT:PSS modification by other solvents could lead to morphological rearrangements, i.e., unfavorable reshuffling of PEDOT and PSS chains and enhanced phase separation of PEDOT and PSS with an undesired distribution of insulating PSS within or on top of the film. All these issues could potentially cause an energy barrier.[80,89] Prosa et al. documented a facile and reproducible procedure, eliminating the consecutive and multiple-layer deposition of PEDOT:PSS.[90] From a suspension containing a nonionic fluorosurfactant (Zonyl FS-300), PEDOT:PSS film was fabricated, aiming to keep similar characteristics as the original untempered formula. The procedure used a simple rinsing of the-then-deposited film with isopropanol, washing out the excess amount of surfactant and PSS. The isopropanol-treated modified PEDOT:PSS, followed by ZnO nanoparticles deposition formed a better-quality ICL for tandem architectures. The modified ICL

demonstrated an outstanding performance without additional interfacial barriers. Rasi et al. established a potent formulation for depositing PEDOT:PSS, while satisfying the requirements of low heat treatment and surface energy at the same stage of fabrication.[91] ZnO nanoparticles on top of PEDOT:PSS were spin coated from isoamyl alcohol to form ICL. They discovered that fabrication of the commercially accessible PEDOT:PSS (Al4083) did not necessarily require any surfactant, because fabrication in inert atmosphere engaging H_2O/1-propanol mixture can provide compatibility over a wide range of photoactive materials. Deprived of additional thermal annealing, not only did they successfully fabricate double-junction tandem devices but also triple-junction tandem solar cells having different functional materials. Moreover, they utilized the same methodology to fabricate a solution-processed quadrupled-junction polymer tandem solar cell carrying complementary absorbing layers.[92] Their experimental results revealed that bimolecular recombination in active material layer hinges the efficiency of the quadrupled-junction device.

Constructing OTSCs via fabricating photoactive material layers, indeed, requisitely demands orthogonality of the corresponding solvents. Avoiding compatibility of the solutions and staying in tune with such strict requisition, one can fabricate a subcell unit on top of another by stamping. Ka et al. adopted stamping methodology, eliminating solution requirements.[93] The top subcell utilizing small-molecule BHJs was first fabricated via spin coating over poly(dimethylsiloxane) (PDMS) stamp and subsequently dried at high-vacuum-eliminating additives. Then, the top subcell was transferred to the bottom subcell on ITO by stamping after mild temperature annealing, governing conformal interaction at the interface. The measured V_{OC} for OTSCs was nearly equal to the summed V_{OC} of the subcells; however, the device revealed low efficiency due to low FF. Continued work by the same author (Ka) demonstrated a polymer-based OTSC.[94] Herein, they successfully utilized stamp transfer method for depositing both P3HT:PC$_{60}$BM as top and PCPDTBT:PC$_{70}$BM as bottom subcell stacks, whereas bathocuproine (BCP):Ag/Ag-islands/HAT-CN as ICLs was done via thermal evaporation. The OTSCs displayed an almost identical V_{OC} when the individual V_{OC}s of the subcells were summed up, whereas the obtained FF stayed at 0.60. Che et al. followed the identical methodology for fabricating bottom subcell by thermal

evaporation and deposited top subcell by solution processing.[95] The top subcell consisted of PTB7-Th:BT-CIC and was directly fabricated through spin coating over the thermally evaporated bottom cell, which comprised DTDCPB:C_{70}, subsequently coated with thermally evaporated BPhen:C60/Ag functioning as ETL and PEDOT:PSS as HTL. The OTSC devices achieved a tremendously high PCE of 15%, gathering a high EQE between 70% and 80%. The obtained J_{SC} corresponded to 12.7 mA cm^{-2}, which was further improved to 13.3 mA cm^{-2} by coating with an antireflecting agent using glass facade. Furthermore, V_{OC} showed similarities to the summed V_{OC} of the stacked subcells and the FF approached as high as 0.71. Remarkably, large-area fabrication carrying active material at 2 and 9 mm^2 dimensions still retained a high PCE for a number of 130 devices.

6. Light Management of OTSCs

The architecture of OTSCs features multilayers of individual functional materials. To achieve the optimized performance in OTSCs, understanding of light distribution inside the OTSCs becomes necessary. In other words, fabricating tandems with the optimum thickness of distinct layers of material is mandatory to harvest the most photons from solar spectrum. The scientific community has documented a number of references to acknowledge the balance of light-harvesting ability regarding thickness in fabricating tandems. Earlier, Chen and coworkers documented the first paper by calculating the light distribution of triple-junction organic solar cells (OSCs) by the transfer matrix method. They demonstrated that the thickness of ICL is also critical to the light absorption of different subcells. They successfully fabricated an efficient triple-junction OTSC, introducing three different electron-donating materials having different energy bandgaps, blended with fullerene derivatives. To enhance current matching, they carefully chose materials with bandgaps in the order 1.9, 1.58, and 1.4 eV. They fabricated highly efficient triple-junction OTSCs, delivering a PCE of 11%.[57] Zuo et al. demonstrated the correlation between the thickness of Ag (8–14 nm) in MoO$_3$/Ag/PFN-based ICL and the photocurrent output from the subcells in tandem.[42] The authors described the formation of optical microactivity between Ag layer and Ag contact on the top subcell (shown in **Figure 7**). As a result,

a high PCE of 11% was revealed, while ensuring an elevated summed EQE peak value exceeding 90%.

In observing parallel tandem architecture, the identical photocurrent is not obligatory as both the subcells summed up the individual current in comparison with the configuration with series connection. However, parallel connections are less flexible as voltage can be restrained at the subcell with a lower value of voltage. In constructing single-junction architectures from organic semiconducting materials (with restrained charge carrying abilities), an ideal thickness for fabrication is determined by the balance between charge generation and corresponding bimolecular recombination. While working on optimization of the thickness of material layers, Lee et al. launched theoretical and experimental analysis concerning thickness of MoOx and realizing optical and electrical characteristics.[96] Their ICL contained MoO$_3$/Ag/MoO$_3$ as an intermediate electrode linking top and bottom subcells in parallel connection. The authors described that the photogenerated current in both top and bottom subcells depended on thickness variation of MoOx layer, with varied interference effect concerning bottom cell and with varied microcavity resonance effect for top subcell. Such a phenomenon was also observed by Zuo et al., by introducing an ICL composed of PEDOT:PSS/Ag/Au/MoO$_3$, facilitating an Ohmic contact with both subcells in parallelly connected OTSCs.[97] Following the simulated guidelines, the experimental results observed a profound optical microcavity in the top subcell, which eventually enhanced photon-to-electron response. They fabricated efficient parallel-connected OTSCs, which responded with 11.1% PCE. Besides working on the thickness of the active layers to trap more light, Mantilla-Perez et al. introduced a four-terminal architecture.[98] They deposited the PTB7:PC$_{71}$BM blend as an active material in both subcells while separated by SiO$_2$ dielectric spacer, eliminating the application of an ICL. In addition, the configuration involved coating of ITO on two faces of the glass substrate, to be used for bifacial illumination. Furthermore, the ZnO nanoparticles were synthesized from the simple stirring of zinc acetate dehydrate and ethanolamine in 2-methoxyethanol. The results generated from experimental data were in good agreement with that of numerically predicted data. Finally, the fabricated OTSC devices with an optimal configuration disclosed a PCE of 6.5%. Zuo et al. presented a serially connected tandem configuration with an optically enhanced top
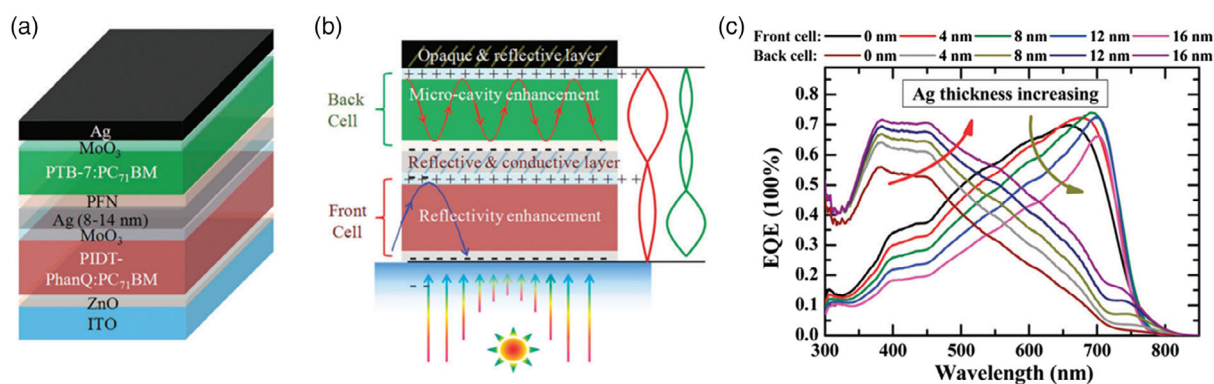

Figure 7. OTSCs with microcavity. a) Device configuration. b) Representation of the microcavity effect in the top subcell. c) Displayed EQE variation dependent on thickness of Ag layer deposition in the ICL. Reproduced with permission.[42] Copyright 2015, The Royal Society of Chemistry.
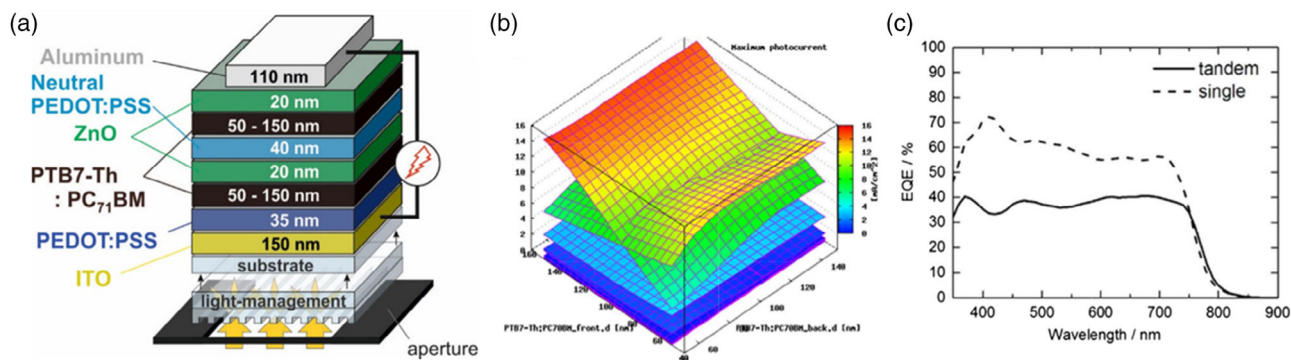
**ADVANCED
SCIENCE NEWS**
www.advancedsciencenews.com

**ADVANCED
ENERGY & SUSTAINABILITY
RESEARCH**
Open Access
www.advenergysustres.com

Figure 8. Schematic representation of a) a tandem cell with an additional light management structure. b) 2D simulation plot of the thickness-dependent photocurrent in top and bottom subcells. c) EQE curves. Reproduced with permission.[100] Copyright 2018, Optical Society of America.

electrode.[99] They introduced a transparent layer of $MoO_3/Ag/TeO_2$ functioning as top electrode to present a dielectric–metal–dielectric (DMD) characteristic.[96] The DMD layers can achieve high transparency with reduced parasitic absorption due to their microcavity configuration. A PCE of 7.4% was established for serially connected ITO-free OTSCs.

Enhancing the optical absorption using active materials without sacrificing the PCE with respect to the thickness of the active material layers in tandems is very challenging. To overcome or minimize this problem, Mayer et al. fabricated homo-OTSCs from non-halogenated solvents by doctor blading.[100] Their optimal technique included a periodical template structure, which was applied externally on the glass side of an ITO-based tandem solar cell. Large-area periodic templates can enhance a selected absorption region. The authors reported enhanced light management with the obtained PCE from 8.7% to 9.5% (shown in **Figure 8**). Mertens et al. designed a homo-tandem architecture, presenting charge carrier generation independency to the incident photons up to a certain angle.[101] Results obtained from simulations and experiments revealed that the constant effective photocurrent in OTSCs was less sensitive to the angle of incident photons while considering illumination up to 65°. The article also explained that the simulated and experimental EQE spectrum varied with respect to angle, whereas the integrated J_{SC} slightly changed considering individual subcells. Recently, Luo et al. introduced a simple and cost-effective strategy for depositing conductive polymeric materials as electrodes in fabricating tandems.[102] While considering the top electrode, the authors used a transparent and highly conductive PEDOT:PSS with additional reflective characteristics, which are beneficial for light management. Their engineered devices enhanced PCE values from 7.23% to 8.34%, corresponding to the thickness variation and light management of PEDOT:PSS.

7. Engaging Photoactive Materials in Constructing OTSCs

In exploiting highly efficient OTSCs, the engineered materials with different bandgaps having complementary selective absorption are crucial. In case of single-junction solar cells, bimolecular recombination potentially limits their thickness. Photoactive materials with thickness-insensitive characteristics with appropriate

blend morphologies can potentially overcome the spectral overlap and eventually achieve enhanced photocurrent for subcells. Moreover, both subcells should be engineered with minimal energy loss from bandgap to V_{OC} to achieve high V_{OC} for tandem architectures.

7.1. Engaging Fullerenes as Electron-Accepting Materials in OTSCs

In engineering single-junction solar cells and tandem devices, traditionally, the most attractive electron acceptor candidate is PCBM due to its isotropy while considering a number of polymeric electron donors as the photoactive blend partners. Previously, a low-bandgap polymer PTB7-Th sets the benchmark as the donor candidate in blending with fullerenes for single-junction devices. Recent documentation revealed around 10% PCE for PTB7-Th/PCBM blends and pronounced efficiency of 10.8% was achieved with $PCB_{71}M$ under the influence of binary solvent additives.[103,104] Li et al. constructed a tandem architecture via doctor blading under ambient environmental conditions.[105] The authors introduced a commercially available polymer GEN-2 in the bottom subcell, whereas PTB7-Th as an active absorber in the top subcell. PEDOT HIL3.3 and ZnO were implemented as ICL, with an extra layer of PEI incorporated between the top subcell and ZnO to guarantee a high FF. Finally, optimization of OTSCs yielded an elevated PCE of 10.03%, with a maintained high FF of 76.6%. Similarly, implementation of the PTB7-Th/$PCB_{71}M$ blend into homo-tandem configurations correspondingly yielded 11.3% PCE, carrying novel HTL.[35] Zheng et al. developed a tandem device by combining two donor polymers, i.e., PDCBT (bottom subcell) and PBDT-TS1 (top subcell), subsequently blended with $PC_{70}BM$ and $PC_{60}BM$, respectively.[21] Both the photoactive absorbers in single-junction devices retained around 70% EQEs while sustaining a V_{OC} of 0.8 V. Moreover, the authors introduced ZnO nanoparticles modified by PFN in combination with MoO_3 as an ICL, which is followed by an ultrathin layer of Ag to establish Ohmic contact between the layers of nanoparticles. Finally, the optimal tandems presented an outstanding PCE of 10.2% with V_{OC} of 1.60 V, J_{SC} of 11.65 mA cm^{-2}, and FF of 54.47%. Considering industrialization for OPV technology, the solution processability on plastic substrates and particularly its stability

by means of UV light exposure for its operation is cardinal. Adams et al. reported an inverted configuration, keeping the blend P3HT-PC$_{60}$BM as the bottom layer absorber and the complementary absorbing organic based on PDPP5T-2 blended with PC$_{70}$BM as the top cell contender.[106] The fabricated tandems demonstrated a PCE of 11% with a wonderful device operational stability of 2000 h. Similarly, Silva et al. engineered a tandem architecture which involved a blend of PCDTBT:PC$_{70}$BM in the bottom cell and PBDTT-DPP:PC$_{71}$BM in the top subcell.[51] This fully solution-processed tandem junction provided a PCE of 9% with a low J_{SC} value of 8.53 mA cm^{-2}, a good V_{OC} (1.60 V), and admirable FF of 66.14%. Zheng et al. documented a newly developed low-bandgap SCP, carrying DPP core and two thiophenic molecules bearing fluorine atoms (PDPP4T-2F).[107] This modified version of DPP-based polymers (PDPP4T-2F) featured a slight broadening in photo-flux absorption, approaching 900 nm, and a deep-lying HOMO energy level advantageously generated high V_{OC} when fabricated with PC$_{60}$BM as an acceptor. Due to the high V_{OC} as well as EQE of the subcells, a remarkable efficiency of 11.62% was achieved for the tandem devices.

Development of benzo[1,2-b:4,5-b′]dithiophene (BDT) is important in engineering novel polymers, attributed to its coplanar architecture with flexible energy levels. Duan et al. reported double-alkylated thiophene-substituted BDT core, sequentially copolymerized with fluorinated benzothiadiazole (BT) flanked with thiophene and furan units.[108] Among these polymers, BDT-FBT-2T gathered further attention due to its ideal bandgap (1.72 eV) and excellent performance even at 250 nm thickness of the active layer when blended with PC$_{70}$BM. Following these features, the authors fabricated a tandem device by adjusting it in the bottom subcell and PMDPP3T blended with PC$_{60}$BM as top subcell absorber. The fabricated tandem devices achieved 8.9% efficiency with limited V_{OC} of 1.42 V caused by significant photon energy loss. Continuing with the quest of exploring BDT core, Guo et al. copolymerized an electron-deficient unit thiazolo[5,4-d]thiazole (TTz) with the BDT core and synthesized wide-bandgap polymer (1.97 eV) PTZ1.[109] PTZ1 carrying deep HOMO energy levels can potentially generate high V_{OC} with the value of 1.01 V when blended with PC$_{70}$BM in single-junction OSCs. Utilizing PTZ1 as the bottom cell absorber and a low-bandgap absorber PBDTTT-C-T blended with PC$_{70}$BM stacked as the top subcell, authors documented a PCE of 10.3% having a perfectly summed-up V_{OC} of 1.65 V with consistent FF of 65% and J_{SC} of 9.6 mA cm^{-2}. Song et al. successfully manufactured wide-bandgap polymers P1 and P2 with attractive deep HOMO energy levels of −5.43 and −5.50 eV, respectively.[110] The deep energy levels ensured high V_{OC} (1.00 V) for these polymers with a blend of PC$_{70}$BM in single junctions. Tandem architectures were constructed by keeping these wide-bandgap polymers as bottom subcell absorbers, and low-bandgap PTB7-Th:PC$_{70}$BM composition was utilized in the top subcell. The tandems constructed of the earlier-mentioned compositions revealed a summed V_{OC} of 1.64 and 1.72 V for polymers P1 and P2, respectively. The fabricated devices delivered an enhanced PCE of 11.42% with J_{SC} of 10.1 mA cm^{-2} for P1-based tandem and 10.05% with 9.3 mA cm^{-2} for P2-based tandem. The lower J_{SC} of P2 tandem could be attributed to the declined EQE of the subcells.

In designing novel polymer materials, the strategies usually include alternative donor and acceptor concepts. Further, to achieve high mobilities, one strategy is to synthesize coplanar, conjugated, and fused aromatic building blocks with flexible energy levels. Ma et al. synthesized copolymers featuring ladder-type indacenodithiophene (IDT) as donor and di-alkoxy-substituted BT as an accepting unit bridged with thiophene (T) and thieno[3,2-b]thiophene (TT) forming PIDTBTO-T and PIDTBTO-TT.[111] Engaging the latter polymer:PC$_{70}$BM with optimized morphology, an efficiency of 8.15% with V_{OC} of 0.91 V was displayed. Convinced by high voltage, the authors kept this wide-bandgap polymer as bottom cell material whereas PTB7-Th:PC$_{70}$BM made it to the top subcell absorbing near-IR photons. The OTSCs nourishing these photoactive absorbers contributed to 11.2% PCE with an elevated V_{OC} of 1.70 V. As very limited literature had studied the flexible and large-area production of OTSCs, Mao et al. investigated tandem architectures with scaled-up device strategies.[112] Their tandem configurations included P3HT:ICBA and PTB7-Th:PC$_{61}$BM. The summarized data attained from their flexible and large-area devices (10.5 cm^2) demonstrated superior efficiency of 6.5%, which is 82% of the PCE offered by reference cells constructed of small area (**Figure 9**).

7.2. Engaging Nonfullerenes as Electron-Accepting Materials in OTSCs

The photoactive layers of OTSCs are often composed of polymer donors and fullerene acceptors, more precisely PC$_{71}$BM/ PC$_{61}$BM. Extensive study has been documented regarding functionalized fullerene derivatives as electron acceptors. In addition to the good performance of fullerene derivatives, they also suffer numerous shortcomings which should be addressed. Primarily, the limited bandgap tunability of fullerene derivatives can cause insufficient photon harvesting ability and potentially low J_{SC}. Followed by the high photovoltage losses in fullerene systems,[113] single-junction architectures often displayed a low V_{OC} ranging from 0.6 from 1.0 V,[114,115] whereas OTSCs can only offer V_{OC} ranging from 1.2 to 1.8 V.[39,116] Finally, annealing fullerenes at elevated temperatures can direct an aggregation governing morphological defects, which can eventually reduce the life span of the devices. The current and most recent research regarding OTSCs mainly revolves around the exploration of novel designs possessing suitable fundamental characteristics. Modern synthetic tools have enabled researchers in engineering novel structures with fused and nonfused cores and attaining desirable molecular entities with flexible optical and electrical characteristics. In this segment, we emphasized on summarizing the recent results documented by researchers globally, focusing on OTSCs from 2015 till date, engaging nonfullerene acceptors (NFAs). In contrast to fullerene-based accepting moieties, NFAs showed efficient charge separation even at reduced energy offsets between the energy levels of donors or acceptors, making them attractive for OTSCs.[117–120]

Liu et al. successfully delivered the first example of fabricating OTSCs composed of nonfullerene components via solution processing.[121] They fabricated the inverted devices using P3HT: SF(DPPB)$_4$ and PTB7-Th:IEIC as the bottom and top subcells.
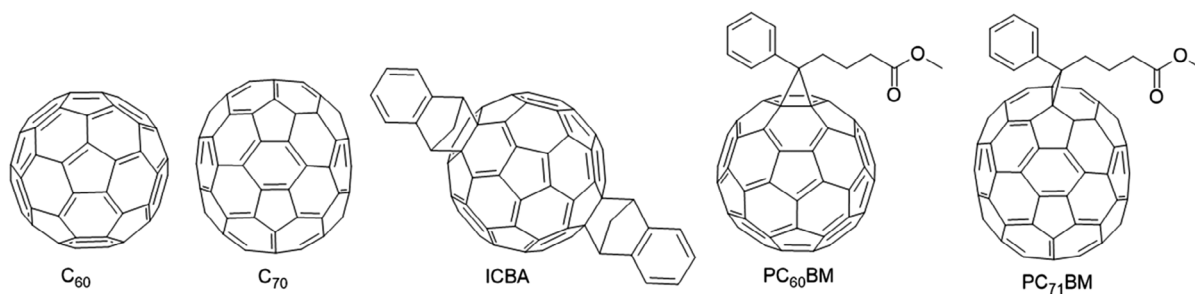
Figure 9. Fullerene-based acceptors used in OTSCs.

Both of the systems referred complementary absorptions with the high potential of gaining elevated V_{OC}. The authors also revealed the potential of NFA-based OTSCs in producing a higher photovoltage, which was advantageous for solar-to-fuel applications and solar-energy-driven water splitting as well. By optical simulations, they finely tuned the thickness of each individual cell and the optimized device approached a PCE of 8.48% with a superb V_{OC} of 1.97 V. V_{OC} submitted by the first subcell was 1.11 V, whereas the second subcell delivered 0.95 V. However, reduced FF governed the decrease in performance. In addition, they conducted a solar-cell-driven water-splitting experiment using OTSCs, which resulted in evolution of H_2 and O_2, demonstrating great potential for solar-to-fuel research applications. Chen et al. demonstrated OTSCs, which utilized P3TA as the donor component having a bandgap of 1.72 eV and SF-PDI$_2$ as the NFA acceptor component having a bandgap of 2.07 eV.[88] To better harvest light intensity, they established a homo-tandem device, presenting a low voltage loss of 0.6 eV. Finally, an efficiency of 10.8% was achieved for tandems with an outstanding V_{OC} of 2.13 V. Continued efforts for developing NFA systems with structural assortments and their implementation into tandem architectures further stimulated device performances. Shi et al. synthesized novel NFAs by introducing thiophene-thieno[3,2-b]thiophene-thiophene (4 T) as the central companion functioning as the donor moiety, terminally flanked with 3-(dicyanomethylidene)indan-1-one (IC), yielding 4TIC.[122] In comparison with the benchmark NFA, the ITIC and 4TIC revealed significantly a narrow bandgap of 1.41 eV with deeper LUMO energy levels. Fabricated single-junction solar cells by integrating a blend of PTB7-Th with 4TIC disclosed a PCE of 10% with superb J_{SC} of 18.4 mA cm^{-2}. Such an attractive J_{SC} suggested 4TIC as an ideal candidate to be utilized as top subcell absorber in constructing tandems. The authors fabricated NFAs-based tandems, carrying PBDB-T:ITIC in the bottom subcell capable of generating a J_{SC} of 16.1 mA cm^{-2} with a high FF (71%) and desirable V_{OC} (.92 V). The OTSCs realized an efficiency of 12.6% with an attained V_{OC} of 1.65 V and J_{SC} approached to 10.6 mA cm^{-2}. In an analogous frame of time, Zuo et al. emphasized on parallel-connected tandem configurations, in which the active absorbers included ITIC and 4TIC as electron acceptors and PTB7-Th as an electron donor.[97] Using a parallel tandem architecture, the tandem devices based on PTB7-Th blended with 4TIC responded with a high PCE of 11.20%, whereas the PTB7-Th:ITIC blend showed a tandem efficiency of 10.22%.

Cheng et al. implemented a simple methodology to establish an equilibrium between the voltage–current trade-off in OTSCs, the authors formulated the top subcell with mixed NFAs.[123] This new strategy included PBDB-T having a wide bandgap of 1.85 eV, blended with NFA IT-M and carrying a medium bandgap of 1.63 eV, and constructed as the bottom cell. The top subcell blend contained PTB7-Th with a medium bandgap of 1.63 eV and two narrow-bandgap NFAs FOIC and F8IC, presenting bandgaps of 1.33 and 1.29 eV, respectively. The bottom subcell individually generated an average V_{OC} of 0.91 V and an attractive J_{SC} (mA cm^{-2}) with improved FF (71.4%) and preserved PCE of 10.6%. The fabricated top subcells were constructed with compatible NFAs and functionally loaded with four extra fluorine atoms, which ultimately down shifted the energy levels, i.e., LUMO with the value of 0.08 eV and HOMO with 0.04 eV, eventually condensing the bandgap by means of 0.04 eV. Due to varied concentrations of both NFAs in the top subcell, the LUMO offset between the two NFAs altered V_{OC} from 0.67 to 0.75 V. Similarly, varied optical bandgaps potentially provoked J_{SC} from 20.5 to 22.7 mA cm^{-2}. Finally, the tandem architectures carrying mixed combination (FOIC: F8IC = 50/50) accomplished an enhanced efficiency of 13.3%.

For constructing highly efficient tandems, the active layers should provide high J_{SC} along with elevated EQE. In addition, the development of near-IR-absorbing photons organics with low energy loss is essential. Moreover, the challenges regarding sophisticated fabrication and the redistribution of optical balance between the individual subcells are mandatory. Chen et al. constructed NFAs T1, T2, T3, and T4, with fluorinated regioisomeric backbones in common.[124] All the NFAs followed a tailored regioisomeric skeleton, receiving IDT as the central component, π-bridged with fluorothieno[3,4-b]thiophene (FTT), trailed by an unsymmetrical approach (proximal vs distal), and are terminally flanked with 1,1-dicyano-methylene-3-indanone (IC). Interestingly, the NFAs exhibited near-IR spectral coverage with slight variation by means of energy modules. The single-junction devices prepared by blending PTB7-Th with these NFAs revealed improved performance attributed to the transformation from distal to proximal construction. Considering all identical molecular formulas, the derivative T2 (also known as IFIC-i-4F) with a bandgap of 1.30 eV displayed a PCE of 10.10%. The optimized single junctions with 1% CN additive showed an impressive EQE approaching 0.81 with a PCE of 10.87% and a superb J_{SC} of 24.85 mA cm^{-2}. The tandem architecture comprising this blend in the top subcell and a blend of PBDB-T: ITIC in the

**ADVANCED
SCIENCE NEWS**

www.advancedsciencenews.com

**ADVANCED
ENERGY & SUSTAINABILITY
RESEARCH**
Open Access
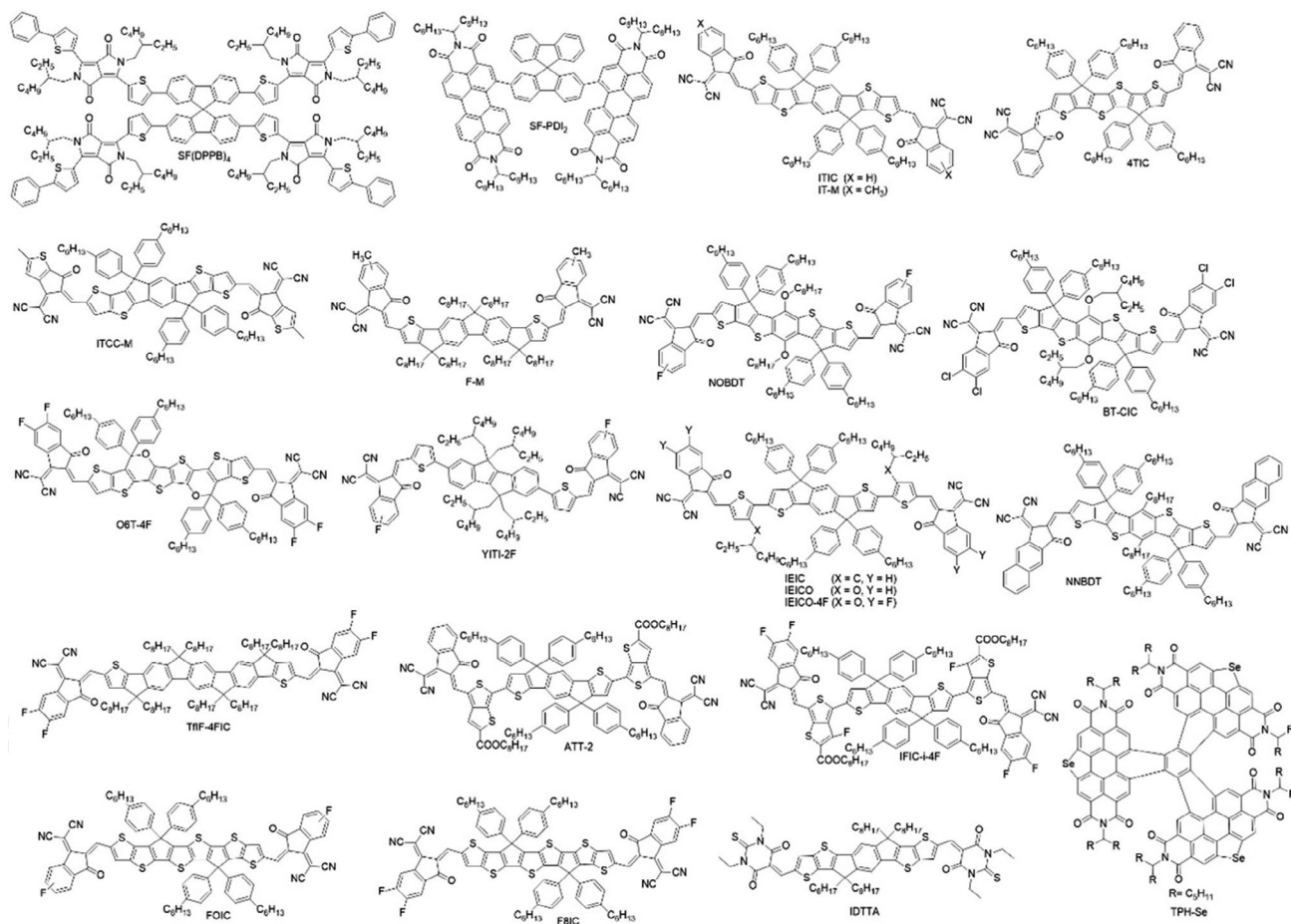
www.advenergysustres.com

Figure 10. Small-molecular acceptors discussed in this article.

bottom subcell established a noteworthy efficiency of 14.64% with a V_{OC} of 1.56 V, a suitable J_{SC} of 13.22 mA cm^{-2}, and FF of 71% (**Figure 10**).

Achieving high efficiencies for OTSCs involving NFAs renders to the obstacle regarding precise bandgap engineering (ranging between 1.5 and 1.6 eV). Such a bandgap is too narrow to be suitable for bottom subcell for a wide-bandgap absorber and too large for the top subcell for a narrow-bandgap absorber. A solution to the aforementioned impediment, Cui et al. successfully launched an NFA-based active absorber, which is a derivative of ITIC and entitled as ITCC-M. ITCC-M presented an appropriate bandgap of 1.68 eV.[36] The single-junction configurations implemented with PBDB-T:ITCC-M blend reflected EQE around 75% with a summarized V_{OC} of 1.03 V and appropriate J_{SC} of 14.5 mA cm^{-2}. The authors used PBDTTT-E-T:IEICO as the top subcell absorber and considered a blend of newly developed NFA in the bottom subcell. The resultant tandem delivered an outstanding efficiency of 13% with a reasonable V_{OC} of 1.79 V and J_{SC} of 11.4 mA cm^{-2}. Finally, the optimized fabrication of OTSCs resulted in tremendous PCEs of 13–14.1% under an illumination of 0.02–1 sun. Continued work by the same research group utilized an appropriate absorber for elevating efficiencies as well as J_{SC}. Later, they presented a blend comprising

wide-bandgap polymer J52-F (or PFBZ) with a bandgap of 1.94 eV and NFA named as IT-M with the presented bandgap of 1.6 eV. The new combination of wide-bandgap and low-bandgap moieties resulted in an enhanced EQE approaching 800 nm and reduced energy loss from 0.69 to 0.64 eV with an up-shifted FF (73%). The top subcell absorbers of IEICO-4F (bandgap of 1.24 eV) blended with PTB7-Th disclosed an extraordinary spectral response over 1000 nm with an elevated EQE over the entire spectral range. The outcomes of tandem devices yielded a striking PCE of 15% with a certified PCE of 14%. The broader spectral range generated significant increase in J_{SC} (13.3 mA cm^{-2}) with an overall FF of 68%. The promising spectral coverage of 1000 nm by IEICO-4 F also attracted other researchers. Shi et al. also implemented PTB7-Th:IEICO-4F blend as the top subcell candidate in constructing tandems.[125] An efficiency of 9.74% for inverted tandem configurations was demonstrated, although the main focus was entitled to the development of an ICL.

Scheming novel materials for tandem architectures meeting the demands of widening solar flux response, reducing thermalization losses, and minimizing transmission losses simultaneously are quite challenging. Considerable attention has been granted to engineer low-bandgap organic materials with

**ADVANCED
SCIENCE NEWS**

www.advancedsciencenews.com

**ADVANCED
ENERGY & SUSTAINABILITY
RESEARCH**
Open Access

www.advenergysustres.com

near-IR solar spectrum coverage, whereas wide-bandgap organics for bottom subcells carrying potentials of elevated J_{SC} and V_{OC} are uncommon. Zhang et al. designed and successfully synthesized two novel NFAs, named as F-M and NOBDT.[116] The former with the bandgap of 1.65 eV was blended with PBDB-T (1.80 eV) and the latter was adopted with PTB7-Th (1.58 eV). The constructed single-junction architectures realized a desirable performance with EQE of about 70%. Adopting a tandem configuration utilizing F-M blend as the bottom subcell and the NOBDT blend as the top subcell, optimized devices presented an outstanding PCE of 14.11% carrying high V_{OC} (1.71) and J_{SC} (11.72 mA cm^{-2}) with a satisfactory FF of 0.70. In the demand of scheming organics with the ability of reassuring both high J_{SC} and V_{OC}, Liu et al. developed a wide-bandgap NFA named TfIF-4FIC with an optical bandgap of 1.61 eV.[27] Structurally it contained a noncyclic fused core and terminally was capped with fluoro-substituted IC units, beneficial in down shifting the energy levels, more precisely the LUMO energy level to −3.96 eV. The single-junction configurations comprised this newly synthesized NFA, blended with PBDB-T-2F (donor), offered a tremendous V_{OC} of 0.98 V with an observable J_{SC} of 17.6 mA cm^{-2}, and concluded a PCE of 13.1%. More importantly, the best-performing device established an energy loss of 0.63 eV. These vital characteristics ensured the bottom cell residency for this combination in tandem architectures, whereas the low-bandgap blend of PTB7-Th:PCDTBT:IEICO-4F was entitled as the top cell contender. The champion OTSCs demonstrated a promising efficiency of 15%, participated by the nearly doubled V_{OC} of 1.60 V, an outstanding J_{SC} of 13.6 mA cm^{-2}, and an acceptable FF of 69%. Considering OTSCs, the challenging part is to maintain a balance between the current densities delivered by individual subcells. Consequently, the alteration of active layer thickness of individual subcells handled delicately is essential. Yue et al. designed new NFAs, comprising indenoindene as the central building block, thiophene as a p-bridge, and is terminally regulated with fluorine atoms.[126] Among these new NFAs ((YITI-0F, YITI-2F, and YITI-4F), YITI-2F owned a medium-bandgap (1.64 eV), single-junction configuration having a blend of PBDB-T:YITI-2F and delivered an efficiency of 10.05%. The authors introduced this scheme as the bottom subcell candidate, whereas a previously documented narrow-bandgap NFA (ATT2) was blended with PTB7-Th and stacked as top subcell partner. Eventually, the tandem configuration produced a significant PCE of 11.9%. A slightly lower PCE value was mainly attributed to the photon energy loss, inferior FF, and reduced EQE intensity presented by individual top and bottom subcells.

Besides designing donating schemes for the bottom subcell in tandems, NFAs with wide bandgaps have to be explored. Very recently, Firdaus et al. synthesized two NFAs, named as IDTA and IDTTA, with optical bandgaps of 1.90 and 1.75 eV, respectively.[127] The newly synthesized NFAs had a central donating core consisting of IDT and IDTT, terminally flanked on both sides with 1,3-diethyl-2-thiobarbituric acid. Both NFAs were blended with the famous donor polymer PBDB-T having an optical bandgap of 1.83 eV to construct single junctions. The devices based on IDTA and IDTTA responded with 7.4% and 10.8% (record PCE for wide-bandgap NFAs) PCEs, respectively. The IDTTA single cell revealed an elevated J_{SC} of 15.8 mA cm^{-2}, high V_{OC} of 0.99 V, and an amazing FF over 71%. With assistance

taken from optical–electrical device modeling, the authors implemented this blend (PBDB-T:IDTTA) in the bottom subcell, whereas PTB7-Th:IEICO-4F supported as the top subcell candidate in constructing tandems. Eventually, the tandem configuration realized a fair V_{OC} of 1.66 V and superb J_{SC} of 13.6 mA cm^{-2}, contributing to a PCE of 15%. An excellent FF of almost 70% was delivered but no EQE data were established. Besides the novel NFA synthesis, novel donor materials loaded with wide bandgaps, strong complementary absorption, and perfectly aligned energy modules are essential. Xu et al. alternatively focused on donor polymeric materials and reported two wide-bandgap (up to 2.10 eV) SCPs PBDT-TDZ and PBDTS-TDZ.[128] The single-junction devices with a blend of PBDTS-TDZ:ITIC, processed from green solvent with no additional treatment, featured a remarkable efficiency of 12.8% with tremendous V_{OC} (1.10 V), low energy loss (0.48 eV), and fantastic J_{SC} of 17.78 mA cm^{-2}. Implementing this material into a homo-tandem configuration entitled 13.4% efficiency with elevated values of J_{SC} (up to 13.35 mA cm^{-2}) and V_{OC} (2.13 V). Meng et al. took synergistic consideration in efficiently tackling complementary absorptions and energy losses through thermalization and ensured high J_{SC} and V_{OC}.[30] The authors reported a tandem architecture which used identical polymer donor material PBDB-T in individual subcells, whereas two NFAs F-M and NNBDT showed complementary absorption. The inverted single-junction configuration with PBDB-T:F-M blend bounced back with 10% efficiency, V_{OC} of almost 1 V, and fantastic J_{SC} of 14 mA cm^{-2}. The PBDB-T:NNBDT blend with fabricated inverted devices delivered a V_{OC} of 0.86, desirable J_{SC} of 20.06 mA cm^{-2}, and overall PCE of 11.87%. Eventually, the fabricated OTSCs consisted of PBDB-T:F-M in the bottom subcell and PBDB-T:NNBDT in the top subcell and produced a PCE of 14.52% with an elevated V_{OC} of 1.82 V, a prominent FF of 74.7%, and an average J_{SC} of 10.68 mA cm^{-2}.

7.3. Engaging Fullerene/Nonfullerene Combination as an Electron-Accepting Material in OTSCs

Tandem configuration usually involved the introduction of wide-bandgap absorbers in the bottom subcell, whereas the top subcell is occupied by low-bandgap semiconducting materials. The former produces high V_{OC} attributed to the potential of short-wavelength photon absorption and the later delivers low V_{OC} due to long-wavelength photon capture, eventually contributing to reduced thermalization loss.[22,129,130] In addition, ternary absorber or quaternary absorber blend system in a single junction is found to be beneficial to reduce thermalization loss due to cascading energy bandgaps. Thus, by involving both fullerene and nonfullerene-based electron acceptors, the absorption of tandem cells can be further improved and thermalization loss can be greatly reduced. Qin et al. introduced a narrow-bandgap NFA, IEICO (optical bandgap: 1.34 eV), as the viable contender with the ability of extended photoresponse surpassing 900 nm.[131] An optimized blend of IEICO with PBDTT-E-T donor polymer in single junctions gave a PCE of 9.32%, accompanied by FF of 64%, V_{OC} of 0.81 V, and a valuable J_{SC} of 17.98 mA cm^{-2}. The authors also fabricated single junctions carrying a blend of PBDD4T-2F:PC$_{61}$BM and PBDD4T-2 F:PC$_{71}$BM, where the

**ADVANCED
SCIENCE NEWS**

www.advancedsciencenews.com

**ADVANCED
ENERGY & SUSTAINABILITY
RESEARCH**
Open Access

www.advenergysustres.com

latter offered an improved J_{SC} (13.67 mA cm^{-2}) and PCE (9.23%) than the former configuration. Subsequently, the blend of PBDTT-E-T:IEICO was entitled in top subcell, whereas the bottom subcell composition combined PBDD4T-2 F with PC$_{71}$BM in tandem configuration. The optimized tandem devices presented an outstanding PCE of 12.80%, with an exactly doubled V_{OC} (1.71 V) of both subcells, a contributed J_{SC} of 11.51 mA cm^{-2}, and FF of 65%.

Till date, the record efficiency for any OTSCs is featuring a ternary blend of polymers/NFAs/fullerene in subcells. Meng et al. documented a tandem configuration involving a combination of photoactive materials, leading to a significantly higher PCE of 17.4% (shown in Figure 3c).[58] The evaluated single-junction devices incorporated a blend of active absorbers, in which the PBDB-T functioned as a donating polymer and F-M an electron-accepting contender. The blended active mixture enhanced photoresponse (up to 720 nm) with a substantially higher J_{SC} of 15.96 mA cm^{-2}, EQE closed to ≈70%, FF of 69.8%, and an attractive V_{OC} of 0.94 V. Such an elevated performance for each section can be accredited to inverted device architecture with optimal morphology. The authors introduced this blend into the bottom subcell in tandem devices, whereas the top subcell contained a blend consisted of ternary absorbing materials of PTB7-Th:O6T-4F:PC$_{70}$BM. The NFA O6T-4F (bandgap: 1.26 eV) can also be recognized as COi8DFIC. The presence of PCBM in the ternary system tempted morphological changes and eventually generated dominant absorption approaching 1050 nm. Finally, the single junctions provided an outstanding J_{SC} of 28 mA cm^{-2}, attributed to the enhanced photo-flux coverage (300–1050 nm), a large V_{OC} of 0.69 V, and a prominent FF (69.7%) with low energy loss of 0.51 eV. Considering these materials with elevated EQEs over a broad spectral range (in single junctions), it also corresponded to a balanced J_{SC} in tandem with the value of 14.2 mA cm^{-2}. This record value of J_{SC} can be attributed to the rearrangement of photo-flux absorbed by the individual cells. In addition, enhanced stabilities were also found by the continuous testing till 166 days, which revealed only 4% degradation. Moreover, large-area tandems (106 mm^2) presented preserved performance of 14.42%. Accomplishing proficient tandem devices, it is mandatory to reduce the absorption overlap, ultimately producing a balanced and higher J_{SC}. Guo et al. developed a strategy which involved polymer absorber PBD1 with an optical bandgap of 1.88 eV.[132] The blend of this wide-bandgap polymer with PC$_{71}$BM as an acceptor presented single junctions with a strong spectral response over 300–650 nm, corresponding to EQE values of 70% over this spectral region. In addition, the device afforded an admirable PCE of 9.8%, whereas J_{SC} values approached 14.6 mA cm^{-2} with an outstanding FF of 74%. Furthermore, the authors engineered a tandem architecture by exploiting this blend in bottom subcell and low-bandgap complementary organics. PTB7-Th blended with IEICO-4F as the top subcell contender. The best fabricated OTSCs presented an outstanding PCE of 14.2% with a rearranged high J_{SC} of 12.3 mA cm^{-2}, V_{OC} of 1.61 V, and a claimed FF of 72%.

Summarizing from the aforementioned, fullerene-based organics and their equivalents were dominant acceptors in OPVs, mainly attributed to their elevated electron mobilities and isotropic charge transport properties.[133,134] However,

synthetic hurdles in modulating energy levels' fullerene-based organics and their blends with corresponding donor moieties limit their further improvement in OSCs.[135,136] Comparing the advantages of NFAs over fullerene-based accepting molecular units, their attractive features included ease of bandgap tunability, which allows more efficient harvesting of the near-IR-region photons for the top subcell. In addition, NFA-based subcells are thermally stable, making them the ideal candidates for the bottom subcell, as the bottom subcell often has to tolerate certain thermal treatment due to the thermal curing of the ICL for improved solvent resistivity.[8]

Finally, a larger energy loss is commonly seen in the fullerene systems contributing to the lower V_{OC} in device performance. The energy loss mainly comes from the driving force required to transfer the electron from donor materials to acceptor materials in the blend system. In other words, a difference in LUMO levels and a difference in HOMO levels between donor and acceptor materials are required for exciton dissociation and commonly regarded as energy loss. In the fullerene acceptor system, the driving force for efficient charge separation can be as large as 0.7 eV.[103,104] In the NFA system, the energy loss can be reduced to 0.6 eV, resulting in an enlarged V_{OC}. Mechanisms have been proposed to explain the low energy loss in NFAs, e.g., extended conjugation, planar backbone, and well-intermixed morphology.[27,36] Each of these factors may help NFAs at some degree to facilitate charge separation for excitons much more efficiently. Thus, the energy loss is mitigated for NFA systems giving enhanced V_{OC}. For some polymer acceptors, when the morphology and energy levels were optimized between donors and acceptors, we can also see small energy loss and large V_{OC}.[41] For ternary blend consisting of both fullerene and NFAs, the energy loss can be further reduced to 0.51 eV, due to the cascaded energy levels helping exciton dissociation.[58]

7.4. Engaging Small-Molecule Donors in OTSCs and All-Polymers OTSCs

Tremendous efforts have been dedicated to engineer novel polymers donors and acceptors including both fullerene and nonfullerene. In addition, limited examples have been documented concerning small-molecule donor blends with fullerenes in developing tandem architectures. Kim et al. applied a blend of small-molecular donors and PCBM in tandem structures.[137] They introduced three small molecules BDTT-(DPP)$_2$-B, BDTT-(DPP)$_2$-F, and BDTT-(DPP)$_2$-CF$_3$, featuring BDT as central core coupled with DPP as an electron-accepting component. Among these small molecules, the optimized single-junction devices carrying a blend of BDTT-(DPP)$_2$-CF$_3$ (bandgap of 1.5 eV):PC$_{70}$BM established 6% efficiency with 0.7 V of V_{OC}. Inverted tandem configurations were used and this blend was used as the top cell candidate, whereas P3HT:ICBA made it to the bottom subcell. Then, fabricated tandems delivered an efficiency of 8.11% with V_{OC} of 1.53 V, a fair FF (68%), and lower J_{SC} of 8 mA cm^{-2}. Zhang et al. entitled three small molecules DR3TSBDT, DR3TBDTT, and DRBDT-TT and implemented them in tandem solar modules.[138] Tandem devices comprised DR3TBDTT:PC$_{71}$BM and DRBDT-TT:PC$_{71}$BM, both functioning as an active absorber in the bottom subcells, displayed an

efficiency of 10.73% and 10.43%, respectively. Interesting results were gathered by DR3TSBDT (bandgap of 1.74 eV) fabricated with $PC_{71}BM$ and entitled a PCE of 9.5%, an arguable V_{OC} (0.91 V), and J_{SC} of 14.3 mA cm^{-2}. Such attractive characteristics featured this blend into the bottom subcell in tandem configurations, whereas low-bandgap PTB7-Th:$PC_{70}BM$ was appointed as rear subcell candidate. Eventually, the device yielded a striking efficiency of 11.5%, with a moderate FF (65%), high V_{OC} (1.69 V), and normal J_{SC} of 10.51 mA cm^{-2}.

Li and coworkers realized the necessity of delivering active materials with more complementary absorption to predominantly produce an improved and balanced J_{SC} with high device performance.[23] They developed solution-processed OTSCs, composed of aforementioned DR3TSBDT:$PC_{70}BM$ blend as the bottom subcell absorber, whereas the top subcell contained a porphyrin-based small molecule caging a zinc metal (DPPEZnP-TBO) with a bandgap of 1.37 eV and subsequently blended with $PC_{60}BM$. Conclusive results were obtained from the single-junction cell of DPPEZnP-TBO:$PC_{60}BM$ with small photon energy loss and excellent EQE values with complementary absorption over 650–900 nm. These active ingredients with optimized configurations delivered an excellent PCE of 12.5%. Importantly, the authors demonstrated that the performance of these small-molecule OTSCs is barely affected by the thicknesses of both the bottom and top subcells and under different light intensities. Finally, Liu, Chen et al. demonstrated the first ever small molecule used (SMPV1) in homo-tandem solar cells and revealed 10.1% PCE.[45] Due to the striking features of small molecules, i.e., cost-effective synthesis, superior film quality, thermal, and mechanical stability, small-molecule OTSCs are advantageous for large-scale production (**Figure 11**).

Finally, considerable attention is also given to the polymer acceptor. In comparison with polymer donors and fullerene/NFAs, polymer acceptors are more difficult to design and synthesize. Yuan et al. demonstrated the first tandem architecture engaging all polymer blends (polymer donor/polymer acceptor).[139] The authors reported two polymers, P2F-DO with a bandgap of 1.6 eV and functioning as donor polymer and N2200 as an electron acceptor with a bandgap of 1.45 eV. The optimized single-junction devices achieved a PCE of 4.7% with V_{OC} of 0.8 V, whereas absorption coverage approached 800 nm with ≈40% obtained EQE. When all-polymer-inverted tandem configurations were used, both polymers covered the entire UV–vis region. A significantly larger efficiency of 6.70% was achieved with a J_{SC} of 7.31 mA cm^{-2}, an almost double V_{OC} (1.58 V), and identical FF to the reference single junctions. The same research group continued to explore novel polymers for all-polymer tandem architectures. Yuan et al. successfully developed regioregular polymers with a displayed near-IR photoresponse approaching 850 nm, ideal for complementary absorption.[140] Both polymers PBBSB and PBFSF carried BDT as the central donor core, whereas the polymeric backbone included flanked BT and FBT accepting units subsequently connected on either side to the weak donating moiety dithieno(3,2-b;2′,3′-d)-silole (DTS). In tandem configuration, this newly synthesized ternary polymer PBFSF with a bandgap of 1.55 eV was blended with the well-known N2200 as the accepting partner for constructing the top subcell. The bottom cell also combined an all-polymer composition, entitling PTP8:P(NDI2HD-T) with bandgaps of 1.8 and 1.85 eV, respectively. Finally, the all-polymer tandem devices responded with an efficiency of 8.3%, J_{SC} of nearly 8 mA cm^{-2}, a doubled V_{OC} (1.77 V), and a low FF of 59%. Zhang et al. reported an all-polymer tandem with a record efficiency of 11%.[41] The authors manufactured single-junction architectures, introducing a polymer donor PTzBI-Si with bandgap of 1.7 eV and the famous N2200 as an electron-accepting candidate. The fabricated device revealed an enlarged V_{OC} of 0.86 V, an outstanding FF of over 70%, and a sufficient J_{SC} of 15.4 mA cm^{-2}. Subsequently, the authors implemented these photo-absorbing materials into all-polymer homo-tandem
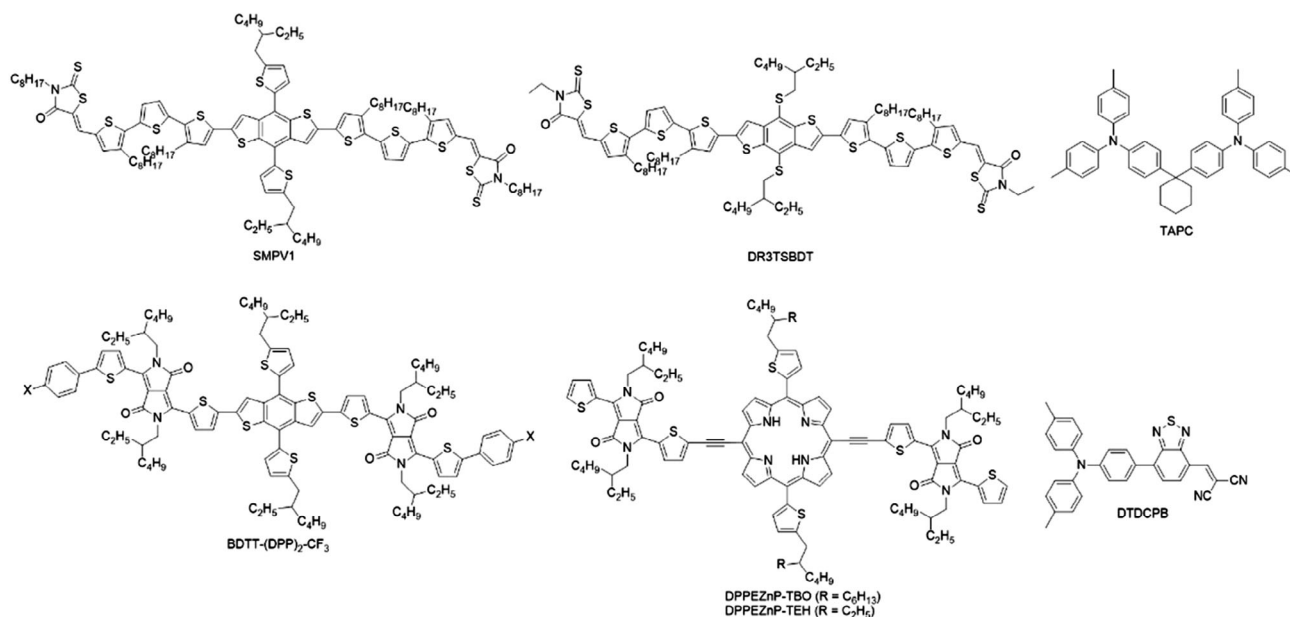

Figure 11. Small-molecular donors.

ADVANCED SCIENCE NEWS
www.advancedsciencenews.com

**ADVANCED
ENERGY & SUSTAINABILITY
RESEARCH**
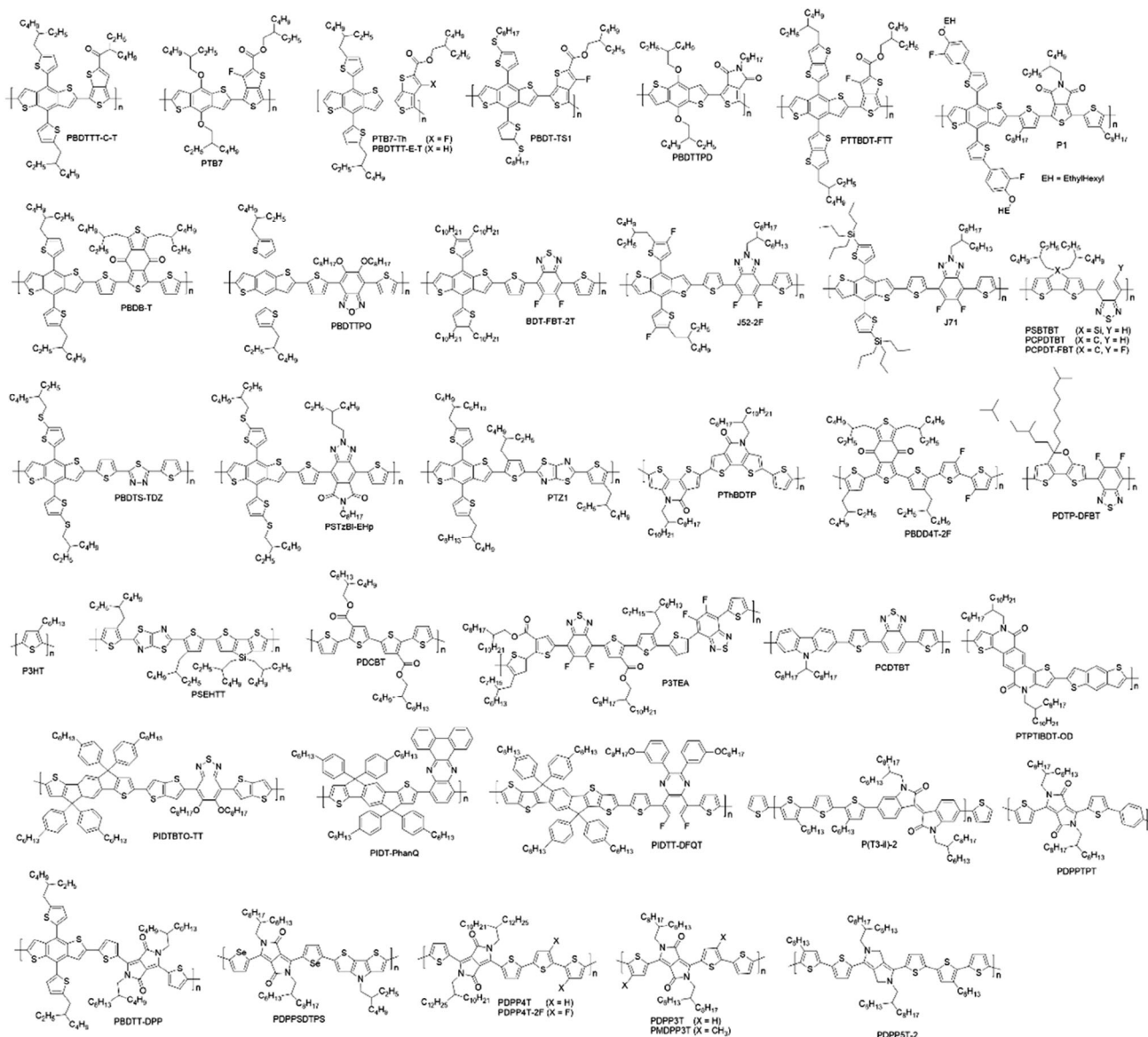Open Access
www.advenergysustres.com

Figure 12. Polymer donor materials used in constructing OTSCs.

configurations, achieving an enhanced spectral response for the devices. Highlights of the results exhibited a limited J_{SC} with the value of 8.6 mA cm^{-2}, n doubled V_{OC} of the single junctions (1.72 V), and an inspirational FF (72%) (**Figure 12**).

8. Organic/Perovskite Combination in OTSCs

The identical characteristics features of solution processability and planar structures carried by both OSCs and perovskite solar cells (PVSCs) made both of them compatible candidates to attain tandem architectures together. Before addressing the fabrication process of OSCs and PVSCs to form tandem architectures, critical difficulties shall be discussed first. First, the availability of perovskite materials revealing ultralow bandgaps (up to 1.3) is

still under developmental stages. Compared with low-bandgap perovskite absorbers, the stabilities of organic active materials (small molecules/polymers) with narrow bandgaps are considerably more stable.[141,142] Thus, the current rational approaches implemented in fabricating organic/perovskite tandems are using low-bandgap organic active materials as the top subcell and wide-bandgap perovskite absorbers as the bottom subcell. Second, the fabrication of top subcell (OSCs) followed by their thermal/chemical treatment could very likely harm the bottom cell (PVSCs). The design of ICL in PVSK/OSC tandem cells requires more consideration in terms of solvent resistivity and orthogonal processing compatibility.

In 2015, Chen et al. illustrated the first hybrid tandem solar cell where two subcells were stacked together with water-/alcohol-miscible PFN/TiO$_2$/PEDOT:PSS as ICL.[143] The top
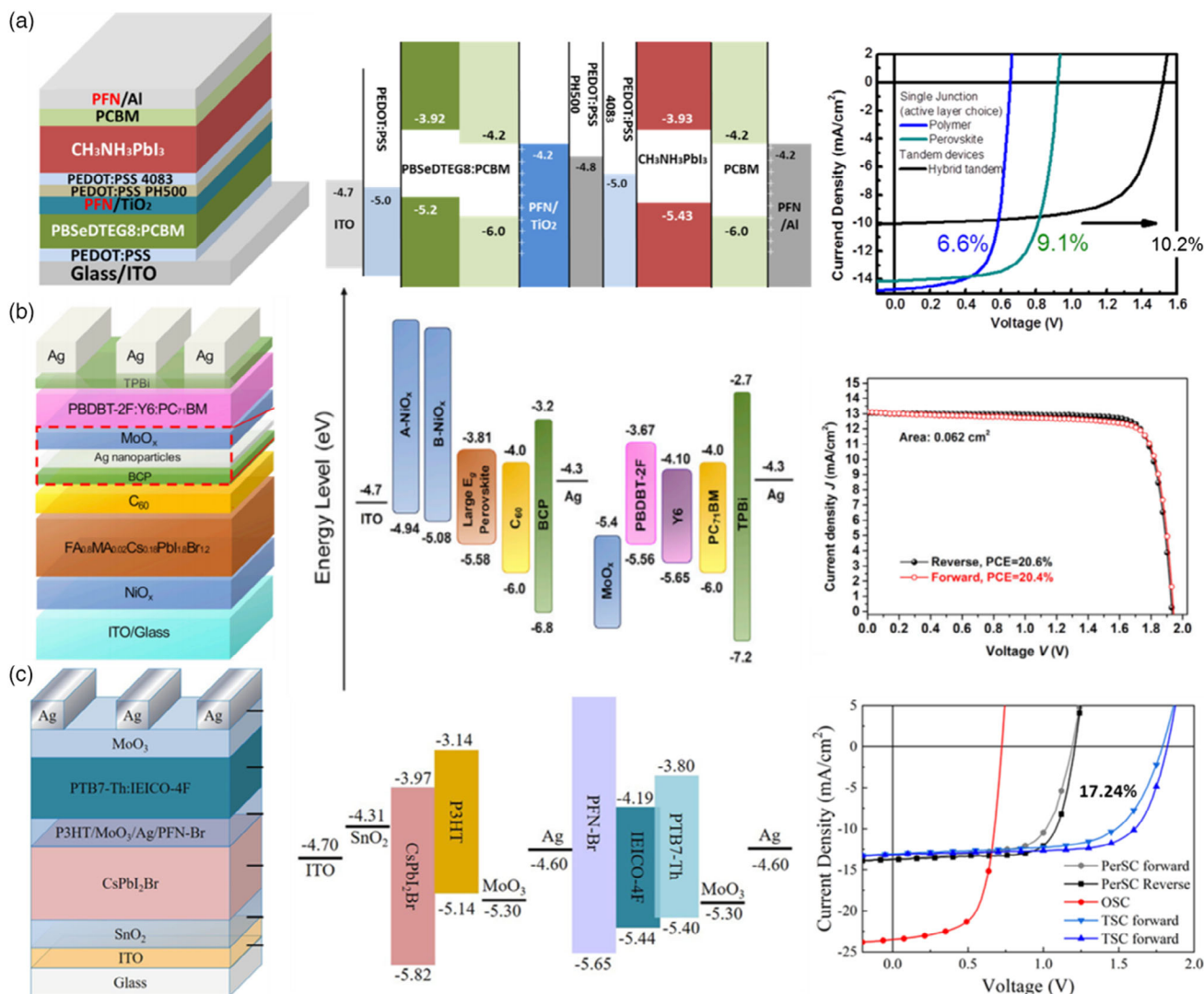
**ADVANCED
SCIENCE NEWS**

www.advancedsciencenews.com

**ADVANCED
ENERGY & SUSTAINABILITY
RESEARCH**
Open Access

www.advenergysustres.com

Figure 13. a) Device architecture representing hybrid tandem solar cell involving MAPbI$_3$ perovskite (top subcell) and polymer absorber (bottom subcell). Reproduced with permission.[143] Copyright 2015, The Royal Society of Chemistry. b) Device architecture representing hybrid tandem solar cell involving perovskite (bottom subcell) and polymer absorber (top subcell). Reproduced with permission.[149] Copyright 2020, Elsevier. c) Device architecture representing hybrid tandem solar cell involving inorganic perovskite (bottom subcell) and polymer absorber (top subcell). Reproduced with permission.[151] Copyright 2020, The American Chemical Society.

subcell carried MAPbI$_3$ perovskite absorber, whereas the bottom subcell was loaded with polymeric IR = sensitive material (PBSeDTEG8) with superb thermal tolerance (shown in **Figure 13**a). Due to the robustness of bottom subcell, a similar ICL with slight modification was used. Finally, the tandem monolithic devices achieved a PCE of 9.13%, which was further enhanced to 10.23%, using PFN as the dipole interlayer. To further improve the performance of hybrid tandem cells, an ultrathin and semitransparent perovskite absorbing layer could be beneficial to allow more light to be harvested by the organic subcell.[144–146] Recently, Liu et al. demonstrated tandem architecture engaging MAPbI$_3$ perovskite absorber ($\approx$90 nm thick) in the bottom subcell, whereas the top subcell contained ($\approx$100 nm thick) polymeric material.[147] Both subcell units were separated by means of a graded ICL comprised of zwitterionic

fullerene (C$_{60}$-SB)/Ag/MoO$_3$ by thermal evaporation to avoid solvent damage. The organic/perovskite tandem devices achieved a maximum efficiency of 16.0% with negligible hysteresis. The engineered devices demonstrated remarkable device metrics and a high V_{OC} of 1.8 V with a desirable FF of 77%.

For harvesting the near-IR and visible region incident photons, tandem architecture should be engineered into the corresponding subcell with specialized material. Liu and coworkers realized perovskite-/organic-based hybrid tandems by an evaporated ICL derived from PFN/Ag (Al)-doped MoO$_3$/MoO$_3$.[148] Sequential deposition was followed for depositing the ICL, and the organic absorber was processed from 1,2-dichlorobenzene (o-DCB) on top of PEDOT:PSS. The perovskite absorber of MAPbI$_3$ was processed with nanostructured-guided morphology, which is a beneficial approach for intimate contact between the

perovskite-PCBM layers via electronic coupling. The perovskite/organic tandem presented a PCE of 8.62% with an FF of 0.68 while carrying a high V_{OC} of 1.58 V attributed to the ignorable energy loss. Recently, Chen and coworkers demonstrated a perovskite/OPV tandem approaching 20% efficiency by tuning the composition of perovskite. Bandgap engineering assisted by optical simulation helped maximize photocurrent output.[149] (shown in Figure 13b)

Recently, Zeng et al. presented a tandem device architecture constructed of all-inorganic perovskite/organic materials.[150] In their communication they introduced a wide-bandgap CsPbI$_2$Br perovskite absorber as the bottom subcell, and the top subcell carried an organic absorber with a ternary component (PTB7-Th:COi8DFIC:PC$_{71}$BM), eliminating spectral overlap and eventually expanding the light harvesting limit up to 1050 nm. The authors claimed 96% retained PCE (15.04%) in nitrogen atmosphere for a duration of 30 days. Lang and coworkers presented CsPbI$_2$Br/OPV tandem solar cells reaching 17.24%. The structure of P3HT/MoO$_3$/Ag/PFN-Br was introduced as a new ICL to facilitate efficient charge recombination and low voltage loss.[151] (shown in Figure 13c)

9. Semitransparent OTSCs

To fulfill the rocketed demands of energy globally, the PV community is implementing their technologies in sunny and remote locations. The current scenario of installing devices in such areas can only harvest a portion of solar radiation. The quest for massive solar light capturing can be enhanced via installation of integrated semitransparent PVs (ST-PVs) covering the surfaces of

automobiles and skyscrapers.[152,153] The perovskites and OPVs are the cardinal candidates to be implemented in ST-PV modules attributed to their merits of band tunability and potential of having high efficiencies over opaque and flexible devices.

Chen et al. successfully demonstrated the first ST-PV tandem architecture by tuning the external appearance and light-conversion features of two near-IR polymeric absorbers blended with PCBM.[154] Their finest semitransparent tandem solar cells exhibited an average transmission of 30% in the visible range with an efficiency greater than 7% (**Figure 14**a–c). Zuo et al. fabricated ST-PV tandem architecture with one perovskite and one OPV absorber in two subcells.[155] They developed efficient ultralarge-bandgap FAPbBr$_{2.43}$Cl$_{0.57}$ PVSCs with E_g = 2.36 eV and implemented this at bottom subcell. They engineered a dual-functioning ICL PC$_{61}$BM/ZnO-NPs/LS-ITO/PEDOT:PSS, with decent electrical contact as well as guarding the device architecture during fabrication as a buffer layer (shown in Figure 14d–f). The top subcell contained a blend of organic absorber (PTB7-Th:6TIC-4F) with selective near-IR absorption approaching 980 nm. The optimized tandem devices represented a balance between thermalization loss and transmission loss. As a result, the tandem ST-PV devices demonstrated an enhanced PCE of 10.7%, while keeping an average transmittance of 52.91% and light utilization efficiency of 5.66%.

10. Conclusion and Outlook

Recent advances in OSC technologies by implementing various device architectures, designing new molecular and polymeric entities, and discovering new morphological control methods
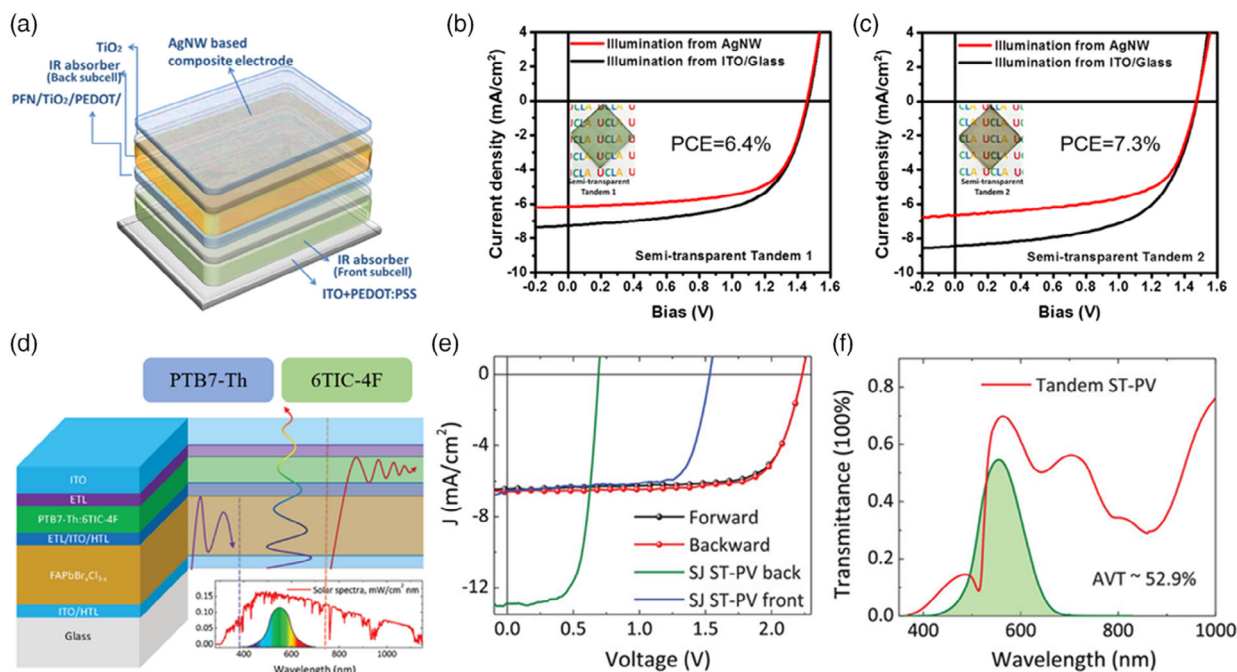

Figure 14. Schematic representation of tandem-structured ST-PV. a) IR polymer tandem ST-PV-based AgNW top electrode. b) J–V characteristic curves representing light-green color tandem cells. c) J–V characteristic curves representing light-brown color tandem cells. Reproduced with permission.[154] Copyright 2013, The Royal Society of Chemistry. d) Hybrid perovskite/organic tandem ST-PV. b) J–V characteristic curves representing hybrid tandem ST-PV. c) Transmission spectra indicating hybrid tandem ST-PV. Reproduced with permission.[155] Copyright 2019, Wiley-VCH GmbH.

have revealed high efficiencies approaching 18.22% for single-junction solar cells. To forecast, we believe that OTSCs will continue to be promising and attractive as they have tremendous capability in developing the next-generation OPV technologies. Theoretical results demonstrate that tandem architectures based on double junctions involving corresponding subcell units with bandgaps of 1.4 and 1.9 eV can accomplish a competitive PCE of 25%, while having an energy offset of 0.6 V and a FF of 80% in both subcells.[141] To develop state-of-the-art OPV technologies with a focus on highly efficient OTSCs (realizing PCE: ≈25%), certain auspicious guidelines for future research are contemplated: 1) robust, orthogonal to solvent corrosion, highly conductive, and transparent ICLs will ensure a high FF and low V_{OC} loss for efficient OTSCs; 2) low-bandgap organics, such as non-fullerene-based acceptors, having decent near-IR and complementary absorption spectra to harvest 1050–1150 nm photons with higher mobilities will be needed for top subcells to provide further photocurrent enhancement for OTSCs; 3) triple-junction tandem design allowing more absorbers to be implemented in OTSCs will further reduce the thermalization loss and boot the efficiency; and 4) light management and simulation by transfer matrix method will be the focus to balance internal light field and output photocurrent, thus maximizing the potential of OTSCs for high efficiency. Furthermore, improved device stabilities involving encapsulation technologies are also cardinal. With the experimental efforts offered by the scientific community around the world, we expect that the continuous development of OTSCs will meet our future needs for energy on different applications, e.g., mobile devices, solar windows, and flexible PV.

Acknowledgements

Conflict of Interest

The authors declare no conflict of interest.

Keywords

[1] S. Sista, Z. Hong, L.-M. Chen, Y. Yang, *Energy Environ. Sci.* **2011**, *4*, 1606.

[2] T. Ameri, G. Dennler, C. Lungenschmied, C. J. Brabec, *Energy Environ. Sci.* **2009**, *2*, 347.

[3] A. Polman, M. Knight, E. C. Garnett, B. Ehrler, W. C. Sinke, *Science* **2016**, *352*, 6283.

[4] Y. Wang, Z. Ren, M. Thway, K. Lee, S. F. Yoon, I. M. Peters, T. Buonassisi, E. A. Fizgerald, C. S. Tan, K. H. Lee, *Sol. Energy Mater. Sol. Cells* **2017**, *172*, 140.

[5] Z. Shi, Y. Bai, X. Chen, R. Zeng, Z. A. Tan, *Sustainable Energy Fuels* **2019**, *3*, 910.

[6] G. Li, R. Zhu, Y. Yang, *Nat. Photonics* **2012**, *6*, 153.

[7] S. B. Darling, F. You, *RSC Adv.* **2013**, *3*, 17633.

[8] P. Cheng, G. Li, X. Zhan, Y. Yang, *Nat. Photonics* **2018**, *12*, 131.

[9] J. Freudenberg, D. Jänsch, F. Hinkel, U. H. F. Bunz, *Chem. Rev.* **2018**, *118*, 5598.

[10] G. Li, V. Shrotriya, J. Huang, Y. Yao, T. Moriarty, K. Emery, Y. Yang, *Nat. Mater.* **2005**, *4*, 864.

[11] F. Padinger, R. S. Rittberger, N. S. Sariciftci, *Adv. Funct. Mater.* **2003**, *13*, 85.

[12] J. Peet, J. Y. Kim, N. E. Coates, W. L. Ma, D. Moses, A. J. Heeger, G. C. Bazan, *Nat. Mater.* **2007**, *6*, 497.

[13] Y. Liang, D. Feng, Y. Wu, S.-T. Tsai, G. Li, C. Ray, L. Yu, *J. Am. Chem. Soc.* **2009**, *131*, 7792.

[14] V. Savikhin, M. Babics, M. Neophytou, S. Liu, S. D. Oosterhout, H. Yan, X. Gu, P. M. Beaujuge, M. F. Toney, *Chem. Mater.* **2018**, *30*, 7872.

[15] J. Hou, H.-Y. Chen, S. Zhang, G. Li, Y. Yang, *J. Am. Chem. Soc.* **2008**, *130*, 16144.

[16] K. Weng, X. Xue, F. Qi, Y. Zhang, L. Huo, J. Zhang, D. Wei, M. Wan, Y. Sun, *ACS Appl. Energy. Mater.* **2018**, *1*, 4686.

[17] Q. Liu, Y. Jiang, K. Jin, J. Qin, J. Xu, W. Li, J. Xiong, J. Liu, Z. Xiao, K. Sun, S. Yang, X. Zhang, L. Ding, *Sci. Bull.* **2020**. *65*, 272

[18] K. Triyana, T. Yasuda, K. Fujita, T. Tsutsui, *Thin Solid Films* **2005**, *477*, 198.

[19] G. Li, C.-W. Chu, V. Shrotriya, J. Huang, Y. Yang, *Appl. Phys. Lett.* **2006**, *88*, 253503.

[20] G. Dennler, M. C. Scharber, T. Ameri, P. Denk, K. Forberich, C. Waldauf, C. J. Brabec, *Adv. Mater.* **2008**, *20*, 579.

[21] Z. Zheng, S. Zhang, M. Zhang, K. Zhao, L. Ye, Y. Chen, B. Yang, J. Hou, *Adv. Mater.* **2015**, *27*, 1189.

[22] J. You, L. Dou, K. Yoshimura, T. Kato, T. Moriarty, K. Emery, C. C. Chen, J. Gao, G. Li, Y. Yang, *Nat. Commun.* **2013**, *4*, 1446.

[23] M. Li, K. Gao, X. Wan, Q. Zhang, B. Kan, R. Xia, F. Liu, X. Yang, H. Feng, W. Ni, Y. Wang, J. Peng, H. Zhang, Z. Liang, H.-L. Yip, X. Peng, Y. Cao, Y. Chen, *Nat. Photonics* **2017**, *11*, 85.

[24] W. Shockley, H. J. Queisser, *J. Appl. Phys.* **1961**, *32*, 510.

[25] A. D. Vos, *J. Phys. D: Appl. Phys.* **1980**, *13*, 839.

[26] P. Cheng, J. Wang, X. Zhan, Y. Yang, *Adv. Energy Mater.* **2020**, *10*, 2000746.

[27] G. Liu, J. Jia, K. Zhang, X. E. Jia, Q. Yin, W. Zhong, L. Li, F. Huang, Y. Cao, *Adv. Energy Mater.* **2019**, *9*, 1803657.

[28] S. Lu, X. Guan, X. Li, W. E. I. Sha, F. Xie, H. Liu, J. Wang, F. Huang, W. C. H. Choy, *Adv. Energy Mater.* **2015**, *5*, 1500631.

[29] M. M. Tavakoli, H. Si, J. Kong, *Energy Technol.* **2020**, *9*, 2000751.

[30] L. Meng, Y.-Q.-Q. Yi, X. Wan, Y. Zhang, X. Ke, B. Kan, Y. Wang, R. Xia, H.-L. Yip, C. Li, Y. Chen, *Adv. Mater.* **2019**, *31*, 1804723.

[31] C. Liu, X. Du, S. Gao, A. Classen, A. Osvet, Y. He, K. Mayrhofer, N. Li, C. J. Brabec, *Adv. Energy. Mater.* **2020**, *10*, 1903800.

[32] W. Zeng, C. Xie, W. Wang, S. Li, X. Jiang, S. Xiong, L. Sun, F. Qin, H. Han, Y. Zhou, *Sol. RRL* **2020**, *4*, 1900480.

[33] C. H. Y. Ho, T. Kim, Y. Xiong, Y. Firdaus, X. Yi, Q. Dong, J. J. Rech, A. Gadisa, R. Booth, B. T. O'Connor, A. Amassian, H. Ade, W. You, T. D. Anthopoulos, F. So, *Adv. Energy. Mater.* **2020**, *10*, 2000823.

[34] S. Lu, D. Ouyang, W. C. H. Choy, *Sci. China Chem.* **2017**, *60*, 460.

[35] H. Zhou, Y. Zhang, C.-K. Mai, S. D. Collins, G. C. Bazan, T.-Q. Nguyen, A. J. Heeger, *Adv. Mater.* **2015**, *27*, 1767.

[36] Y. Cui, H. Yao, B. Gao, Y. Qin, S. Zhang, B. Yang, C. He, B. Xu, J. Hou, *J. Am. Chem. Soc.* **2017**, *139*, 7302.

[37] J. Lee, H. Kang, S. Kee, S. H. Lee, S. Y. Jeong, G. Kim, J. Kim, S. Hong, H. Back, K. Lee, *ACS Appl. Mater. Interfaces.* **2016**, *8*, 6144.

[38] K. Zhang, K. Gao, R. Xia, Z. Wu, C. Sun, J. Cao, L. Qian, W. Li, S. Liu, F. Huang, X. Peng, L. Ding, H.-L. Yip, Y. Cao, *Adv. Mater.* **2016**, *28*, 4817.

[39] K. Zhang, B. Fan, R. Xia, X. Liu, Z. Hu, H. Gu, S. Liu, H.-L. Yip, L. Ying, F. Huang, Y. Cao, *Adv. Energy Mater.* **2018**, *8*, 1703180.

[40] Y. Zhou, C. Fuentes-Hernandez, J. Shim, J. Meyer, A. J. Giordano, H. Li, P. Winget, T. Papadopoulos, H. Cheun, J. Kim, M. Fenoll, A. Dindar, W. Haske, E. Najafabadi, T. M. Khan, H. Sojoudi, S. Barlow, S. Graham, J.-L. Brédas, S. R. Marder, A. Kahn, B. Kippelen, *Science* **2012**, *336*, 327.

[41] K. Zhang, R. Xia, B. Fan, X. Liu, Z. Wang, S. Dong, H.-L. Yip, L. Ying, F. Huang, Y. Cao, *Adv. Mater.* **2018**, *30*, 1803166.

[42] L. Zuo, C.-Y. Chang, C.-C. Chueh, S. Zhang, H. Li, A. K. Y. Jen, H. Chen, *Energy Environ. Sci.* **2015**, *8*, 1712.

[43] A. Martínez-Otero, Q. Liu, P. Mantilla-Perez, M. M. Bajo, J. Martorell, *J. Mater. Chem. A* **2015**, *3*, 10681.

[44] S. Lu, X. Guan, X. Li, W. E. I. Sha, F. Xie, H. Liu, J. Wang, F. Huang, W. C. H. Choy, *Adv. Energy Mater.* **2015**, *5*, 1500631.

[45] Y. Liu, C.-C. Chen, Z. Hong, J. Gao, Y. Yang, H. Zhou, L. Dou, G. Li, Y. Yang, *Sci. Rep.* **2013**, *3*, 3356.

[46] C.-H. Chou, W. L. Kwan, Z. Hong, L.-M. Chen, Y. Yang, *Adv. Mater.* **2011**, *23*, 1282.

[47] D. W. Zhao, L. Ke, Y. Li, S. T. Tan, A. K. K. Kyaw, H. V. Demir, X. W. Sun, D. L. Carroll, G. Q. Lo, D. L. Kwong, *Sol. Energy Mater. Sol. Cells* **2011**, *95*, 921.

[48] S. Bag, R. J. Patel, A. Bunha, C. Grand, J. D. Berrigan, M. J. Dalton, B. J. Leever, J. R. Reynolds, M. F. Durstock, *ACS Appl. Mater. Interfaces.* **2016**, *8*, 16.

[49] T. Becker, S. Trost, A. Behrendt, I. Shutsko, A. Polywka, P. Görrn, P. Reckers, C. Das, T. Mayer, D. Di Carlo Rasi, K. H. Hendriks, M. M. Wienk, R. A. J. Janssen, T. Riedl, *Adv. Energy. Mater.* **2018**, *8*, 1702533.

[50] D. Di Carlo Rasi, P. M. J. G. van Thiel, H. Bin, K. H. Hendriks, G. H. L. Heintges, M. M. Wienk, T. Becker, Y. Li, T. Riedl, R. A. J. Janssen, *Sol. RRL* **2019**, *3*, 1800366.

[51] W. J. da Silva, F. K. Schneider, A. R. b. Mohd Yusoff, J. Jang, *Sci. Rep.* **2015**, *5*, 18090.

[52] A. F. Mitul, L. Mohammad, S. Venkatesan, N. Adhikari, S. Sigdel, Q. Wang, A. Dubey, D. Khatiwada, Q. Qiao, *Nano Energy* **2015**, *11*, 56.

[53] X. Du, O. Lytken, M. S. Killian, J. Cao, T. Stubhan, M. Turbiez, P. Schmuki, H.-P. Steinrück, L. Ding, R. H. Fink, N. Li, C. J. Brabec, *Adv. Energy Mater.* **2017**, *7*, 1601959.

[54] J. You, C.-C. Chen, Z. Hong, K. Yoshimura, K. Ohya, R. Xu, S. Ye, J. Gao, G. Li, Y. Yang, *Adv. Mater.* **2013**, *25*, 3973.

[55] N. M. Torabi, A. Behjat, M. Shahpari, S. Edalati, *J. Nanophotonics* **2015**, *9*, 1.

[56] M. Raïssi, S. Vedraine, R. Garuz, T. Trigaud, B. Ratier, *Sol. Energy Mater. Sol. Cells* **2017**, *160*, 494.

[57] C.-C. Chen, W.-H. Chang, K. Yoshimura, K. Ohya, J. You, J. Gao, Z. Hong, Y. Yang, *Adv. Mater.* **2014**, *26*, 5670.

[58] L. Meng, Y. Zhang, X. Wan, C. Li, X. Zhang, Y. Wang, X. Ke, Z. Xiao, L. Ding, R. Xia, H.-L. Yip, Y. Cao, Y. Chen, *Science* **2018**, *361*, 1094.

[59] S. Lu, X. Guan, X. Li, J. Liu, F. Huang, W. C. H. Choy, *Nano Energy.* **2016**, *21*, 123.

[60] S.-Y. Chang, Y.-C. Lin, P. Sun, Y.-T. Hsieh, L. Meng, S.-H. Bae, Y.-W. Su, W. Huang, C. Zhu, G. Li, K.-H. Wei, Y. Yang, *Sol. RRL* **2017**, *1*, 1700139.

[61] Z. Shi, H. Liu, L. Xia, Y. Bai, F. Wang, B. Zhang, T. Hayat, A. Alsaedi, Z. A. Tan, *China J. Chem.* **2018**, *36*, 194.

[62] S. Esiner, H. van Eersel, M. M. Wienk, R. A. J. Janssen, *Adv. Mater.* **2013**, *25*, 2932.

[63] S. Lu, H. Lin, S. Zhang, J. Hou, W. C. H. Choy, *Adv. Energy Mater.* **2017**, *7*, 1701164.

[64] M. Vasilopoulou, E. Polydorou, A. M. Douvas, L. C. Palilis, S. Kennou, P. Argitis, *Energy Environ. Sci.* **2015**, *8*, 2448.

[65] H. W. Kroto, J. R. Heath, S. C. O'Brien, R. F. Curl, R. E. Smalley, *Nature* **1985**, *318*, 162.

[66] G. Che, B. B. Lakshmi, E. R. Fisher, C. R. Martin, *Nature* **1998**, *393*, 346.

[67] R. He, X. Huang, M. Chee, F. Hao, P. Dong, *Carbon Energy* **2019**, *1*, 109.

[68] H. Zhu, J. Wei, K. Wang, D. Wu, *Sol. Energy Mater. Sol. Cells* **2009**, *93*, 1461.

[69] C.-Y. Chang, W.-K. Huang, Y.-C. Chang, K.-T. Lee, H.-Y. Siao, *Chem. Mater.* **2015**, *27*, 1869.

[70] D. Hecht, L. Hu, G. Grüner, *Appl. Phys. Lett.* **2006**, *89*, 133112.

[71] J. L. Blackburn, T. M. Barnes, M. C. Beard, Y.-H. Kim, R. C. Tenent, T. J. McDonald, B. To, T. J. Coutts, M. J. Heben, *ACS Nano* **2008**, *2*, 1266.

[72] A. S. R. Bati, L. Yu, S. A. Tawfik, M. J. S. Spencer, P. E. Shaw, M. Batmunkh, J. G. Shapter, *iScience* **2019**, *14*, 100.

[73] M. Raïssi, L. Vignau, E. Cloutet, B. Ratier, *Org. Electron.* **2015**, *21*, 86.

[74] R. Kang, S. Park, Y. K. Jung, D. C. Lim, M. J. Cha, J. H. Seo, S. Cho, *Adv. Energy Mater.* **2018**, *8*, 1702165.

[75] M. Li, W. Ni, B. Kan, X. Wan, L. Zhang, Q. Zhang, G. Long, Y. Zuo, Y. Chen, *Phys. Chem. Chem. Phys.* **2013**, *15*, 18973.

[76] Z. Ding, Z. Hao, B. Meng, Z. Xie, J. Liu, L. Dai, *Nano Energy* **2015**, *15*, 186.

[77] A. Ananthanarayanan, Y. Wang, P. Routh, M. A. Sk, A. Than, M. Lin, J. Zhang, J. Chen, H. Sun, P. Chen, *Nanoscale* **2015**, *7*, 8159.

[78] S. Kundu, R. M. Yadav, T. N. Narayanan, M. V. Shelke, R. Vajtai, P. M. Ajayan, V. K. Pillai, *Nanoscale* **2015**, *7*, 11515.

[79] N. T. Ho, T. V. Tam, H. N. Tien, S.-J. Jang, T. K. Nguyen, W. M. Choi, S. Cho, Y. S. Kim, *J. Nanosci. Nanotechnol.* **2017**, *17*, 5686.

[80] C. M. Palumbiny, J. Schlipf, A. Hexemer, C. Wang, P. Müller-Buschbaum, *Adv. Electron. Mater.* **2016**, *2*, 1500377.

[81] A. R. b. M. Yusoff, D. Kim, H. P. Kim, F. K. Shneider, W. J. da Silva, J. Jang, *Energy Environ. Sci.* **2015**, *8*, 303.

[82] J. You, L. Dou, K. Yoshimura, T. Kato, K. Ohya, T. Moriarty, K. Emery, C.-C. Chen, J. Gao, G. Li, Y. Yang, *Nat. Commun.* **2013**, *4*, 1446.

[83] T. R. Andersen, H. F. Dam, B. Andreasen, M. Hösel, M. V. Madsen, S. A. Gevorgyan, R. R. Søndergaard, M. Jørgensen, F. C. Krebs, *Sol. Energy Mater. Sol. Cells* **2014**, *120*, 735.

[84] N. Li, D. Baran, G. D. Spyropoulos, H. Zhang, S. Berny, M. Turbiez, T. Ameri, F. C. Krebs, C. J. Brabec, *Adv. Energy Mater.* **2014**, *4*, 1400084.

[85] Q. Wei, T. Nishizawa, K. Tajima, K. Hashimoto, *Adv. Mater.* **2008**, *20*, 2211.

[86] H. Kang, S. Kee, K. Yu, J. Lee, G. Kim, J. Kim, J.-R. Kim, J. Kong, K. Lee, *Adv. Mater.* **2015**, *27*, 1408.

[87] S. Kim, H. Kang, S. Hong, J. Lee, S. Lee, B. Park, J. Kim, K. Lee, *Adv. Funct. Mater.* **2016**, *26*, 3563.

[88] S. Chen, G. Zhang, J. Liu, H. Yao, J. Zhang, T. Ma, Z. Li, H. Yan, *Adv Mater.* **2017**, *29*, 1604231.

[89] M. Vosgueritchian, D. J. Lipomi, Z. Bao, *Adv. Funct. Mater.* **2012**, *22*, 421.

[90] M. Prosa, M. Tessarolo, M. Bolognesi, T. Cramer, Z. Chen, A. Facchetti, B. Fraboni, M. Seri, G. Ruani, M. Muccini, *Adv. Mater. Interfaces* **2016**, *3*, 1600770.

[91] D. Di Carlo Rasi, K. H. Hendriks, G. H. L. Heintges, G. Simone, G. H. Gelinck, V. S. Gevaerts, R. Andriessen, G. Pirotte, W. Maes, W. Li, M. M. Wienk, R. A. J. Janssen, *Sol. RRL* **2018**, *2*, 1800018.

[92] D. Di Carlo Rasi, K. H. Hendriks, M. M. Wienk, R. A. J. Janssen, *Adv. Mater.* **2018**, *30*, 1803836.

[93] Y. Ka, H. Hwang, C. Kim, *Sci. Rep.* **2017**, *7*, 1942.

**ADVANCED
SCIENCE NEWS**

www.advancedsciencenews.com

**ADVANCED
ENERGY & SUSTAINABILITY
RESEARCH**
Open Access

www.advenergysustres.com

[94] Y. Ka, H. Kim, S. Han, C. Kim, *Nanoscale* **2018**, *10*, 12588.

[95] X. Che, Y. Li, Y. Qu, S. R. Forrest, *Nat. Energy* **2018**, *3*, 422.

[96] S. Lee, T. E. Kang, D. Han, H. Kim, B. J. Kim, J. Lee, S. Yoo, *Sol. Energy Mater. Sol. Cells* **2015**, *137*, 34.

[97] L. Zuo, J. Yu, X. Shi, F. Lin, W. Tang, A. K.-Y. Jen, *Adv. Mater.* **2017**, *29*, 1702547.

[98] P. Mantilla-Perez, A. Martinez-Otero, P. Romero-Gomez, J. Martorell, *ACS Appl. Mater. Interfaces* **2015**, *7*, 18435.

[99] L. Zuo, C.-Y. Chang, C.-C. Chueh, Y. Xu, H. Chen, A. K. Y. Jen, *J. Mater. Chem. A* **2016**, *4*, 961.

[100] J. A. Mayer, T. Offermans, M. Chrapa, M. Pfannmöller, S. Bals, R. Ferrini, G. Nisato, *Opt. Express* **2018**, *26*, A240.

[101] A. Mertens, J. Mescher, D. Bahro, M. Koppitz, A. Colsmann, *Opt. Express* **2016**, *24*, A898.

[102] B. Luo, Y. Jiang, L. Mao, W. Meng, F. Jiang, Y. Xu, Y. Zhou, *J. Mater. Chem. C* **2017**, *5*, 7884.

[103] S.-H. Liao, H.-J. Jhuo, P.-N. Yeh, Y.-S. Cheng, Y.-L. Li, Y.-H. Lee, S. Sharma, S.-A. Chen, *Sci. Rep.* **2014**, *4*, 6813.

[104] Q. Wan, X. Guo, Z. Wang, W. Li, B. Guo, W. Ma, M. Zhang, Y. Li, *Adv. Funct. Mater.* **2016**. *26*, 6635.

[105] N. Li, C. J. Brabec, *Energy Environ. Sci.* **2015**, *8*, 2902.

[106] J. Adams, G. D. Spyropoulos, M. Salvador, N. Li, S. Strohm, L. Lucera, S. Langner, F. Machui, H. Zhang, T. Ameri, M. M. Voigt, F. C. Krebs, C. J. Brabec, *Energy Environ. Sci.* **2015**. *8*, 169.

[107] Z. Zheng, S. Zhang, J. Zhang, Y. Qin, W. Li, R. Yu, Z. Wei, J. Hou, *Adv. Mater.* **2016**, *28*, 5133.

[108] C. Duan, A. Furlan, J. J. van Franeker, R. E. M. Willems, M. M. Wienk, R. A. J. Janssen, *Adv. Mater.* **2015**, *27*, 4461.

[109] B. Guo, X. Guo, W. Li, X. Meng, W. Ma, M. Zhang, Y. Li, *J. Mater. Chem. A* **2016**, *4*, 13251.

[110] S. Song, K. Kranthiraja, J. Heo, T. Kim, B. Walker, S.-H. Jin, J. Y. Kim, *Adv. Energy. Mater.* **2017**, *7*, 1700782.

[111] Y. Ma, S.-C. Chen, Z. Wang, W. Ma, J. Wang, Z. Yin, C. Tang, D. Cai, Q. Zheng, *Nano Energy* **2017**. *33*, 313.

[112] L. Mao, J. Tong, S. Xiong, F. Jiang, F. Qin, W. Meng, B. Luo, Y. Liu, Z. Li, Y. Jiang, C. Fuentes-Hernandez, B. Kippelen, Y. Zhou, *J. Mater. Chem. A* **2017**, *5*, 3186.

[113] K. Vandewal, J. Benduhn, V. C. Nikolis, *Sustainable Energy & Fuels.* **2018**, *2*, 538.

[114] S. Zhang, Y. Qin, J. Zhu, J. Hou, *Adv. Mater.* **2018**, *30*, 1800868.

[115] M. Wang, D. Cai, Z. Yin, S.-C. Chen, C.-F. Du, Q. Zheng, *Adv. Mater.* **2016**, *28*, 3359.

[116] Y. Zhang, B. Kan, Y. Sun, Y. Wang, R. Xia, X. Ke, Y.-Q.-Q. Yi, C. Li, H.-L. Yip, X. Wan, Y. Cao, Y. Chen, *Adv. Mater.* **2018**, *30*, 1707508.

[117] J. Liu, S. Chen, D. Qian, B. Gautam, G. Yang, J. Zhao, J. Bergqvist, F. Zhang, W. Ma, H. Ade, O. Inganäs, K. Gundogdu, F. Gao, H. Yan, *Nat. Energy* **2016**, *1*, 16089.

[118] Y. Li, X. Liu, F.-P. Wu, Y. Zhou, Z.-Q. Jiang, B. Song, Y. Xia, Z.-G. Zhang, F. Gao, O. Inganäs, Y. Li, L.-S. Liao, *J. Mater. Chem. A* **2016**, *4*, 5890.

[119] D. Baran, T. Kirchartz, S. Wheeler, S. Dimitrov, M. Abdelsamie, J. Gorman, R. S. Ashraf, S. Holliday, A. Wadsworth, N. Gasparini, P. Kaienburg, H. Yan, A. Amassian, C. J. Brabec, J. R. Durrant, I. McCulloch, *Energy Environ. Sci.* **2016**, *9*, 3783.

[120] C. Wu, K. Wang, M. Batmunkh, A. S. R. Bati, D. Yang, Y. Jiang, Y. Hou, J. G. Shapter, S. Priya, *Nano Energy.* **2020**, 104480.

[121] W. Liu, S. Li, J. Huang, S. Yang, J. Chen, L. Zuo, M. Shi, X. Zhan, C.-Z. Li, H. Chen, *Adv. Mater.* **2016**, *28*, 9729.

[122] X. Shi, L. Zuo, S. B. Jo, K. Gao, F. Lin, F. Liu, A. K. Y. Jen, *Chem. Mater.* **2017**, *29*, 8369.

[123] P. Cheng, Y. Liu, S.-Y. Chang, T. Li, P. Sun, R. Wang, H.-W. Cheng, T. Huang, L. Meng, S. Nuryyeva, C. Zhu, K.-H. Wei, B. Sun, X. Zhan, Y. Yang, *Joule* **2019**, *3*, 432.

[124] F.-X. Chen, J.-Q. Xu, Z.-X. Liu, M. Chen, R. Xia, Y. Yang, T.-K. Lau, Y. Zhang, X. Lu, H.-L. Yip, A. K.-Y. Jen, H. Chen, C.-Z. Li, *Adv. Mater.* **2018**, *30*, 1803769.

[125] Z. Shi, H. Liu, J. Li, F. Wang, Y. Bai, X. Bian, B. Zhang, A. Alsaedi, T. Hayat, Z. a. Tan, *Sol. Energy Mater. Sol. Cells* **2018**, *180*, 1.

[126] Q. Yue, Z. Zhou, S. Xu, J. Zhang, X. Zhu, *J. Mater. Chem. A* **2018**, *6*, 13588.

[127] Y. Firdaus, Q. He, Y. Lin, F. A. A. Nugroho, V. M. Le Corre, E. Yengel, A. H. Balawi, A. Seitkhan, F. Laquai, C. Langhammer, F. Liu, M. Heeney, T. D. Anthopoulos, *J. Mater. Chem. A* **2020**, *8*, 1164.

[128] X. Xu, T. Yu, Z. Bi, W. Ma, Y. Li, Q. Peng, *Adv. Mater.* **2018**, *30*, 1703973.

[129] L. Dou, J. You, J. Yang, C.-C. Chen, Y. He, S. Murase, T. Moriarty, K. Emery, G. Li, Y. Yang, *Nat. Photonics* **2012**, *6*, 180.

[130] N. Li, D. Baran, K. Forberich, F. Machui, T. Ameri, M. Turbiez, M. Carrasco-Orozco, M. Drees, A. Facchetti, F. C. Krebs, C. J. Brabec, *Energy Environ. Sci.* **2013**, *6*, 3407.

[131] Y. Qin, Y. Chen, Y. Cui, S. Zhang, H. Yao, J. Huang, W. Li, Z. Zheng, J. Hou, *Adv. Mater.* **2017**, *29*, 1606340.

[132] B. Guo, W. Li, G. Luo, X. Guo, H. Yao, M. Zhang, J. Hou, Y. Li, W.-Y. Wong, *ACS Energy Lett.* **2018**, *3*, 2566.

[133] Y. He, Y. Li, *Phys. Chem. Chem. Phys.* **2011**, *13*, 1970.

[134] Y. Ji, L. Xu, X. Hao, K. Gao, *Sol. RRL* **2020**, *4*, 2000130.

[135] Y. Lin, J. Wang, Z.-G. Zhang, H. Bai, Y. Li, D. Zhu, X. Zhan, *Adv. Mater.* **2015**, *27*, 1170.

[136] L. Ye, W. Jiang, W. Zhao, S. Zhang, Y. Cui, Z. Wang, J. Hou, *Org. Electron.* **2015**, *17*, 295.

[137] J.-H. Kim, J. B. Park, H. Yang, I. H. Jung, S. C. Yoon, D. Kim, D.-H. Hwang, *ACS Appl. Mater. Interfaces* **2015**, *7*, 23866.

[138] Q. Zhang, X. Wan, F. Liu, B. Kan, M. Li, H. Feng, H. Zhang, T. P. Russell, Y. Chen, *Adv. Mater.* **2016**, *28*, 7008.

[139] J. Yuan, J. Gu, G. Shi, J. Sun, H.-Q. Wang, W. Ma, *Sci. Rep. 6*, 26459.

[140] J. Yuan, M. J. Ford, Y. Xu, Y. Zhang, G. C. Bazan, W. Ma, *Adv. Energy. Mater.* **2018**, *8*, 1870066.

[141] G. Li, W.-H. Chang, Y. Yang, *Nat. Rev. Mater.* **2017**, *2*, 17043.

[142] N. Torabi, A. Behjat, Y. Zhou, P. Docampo, R. J. Stoddard, H. W. Hillhouse, T. Ameri, *Mater. Today. Energy* **2019**, *12*, 70.

[143] C.-C. Chen, S.-H. Bae, W.-H. Chang, Z. Hong, G. Li, Q. Chen, H. Zhou, Y. Yang, *Mater. Horiz.* **2015**, *2*, 203.

[144] E. Della Gaspera, Y. Peng, Q. Hou, L. Spiccia, U. Bach, J. J. Jasieniak, Y.-B. Cheng, *Nano Energy* **2015**, *13*, 249.

[145] L. Yuan, Z. Wang, R. Duan, P. Huang, K. Zhang, Q. Chen, N. K. Allam, Y. Zhou, B. Song, Y. Li, *J. Mater. Chem. A* **2018**, *6*, 19696.

[146] B. Yang, M. Wang, X. Hu, T. Zhou, Z. Zang, *Nano Energy* **2019**, *57*, 718.

[147] Y. Liu, L. A. Renna, M. Bag, Z. A. Page, P. Kim, J. Choi, T. Emrick, D. Venkataraman, T. P. Russell, *ACS Appl. Mater. Interfaces* **2016**, *8*, 7070.

[148] J. Liu, S. Lu, L. Zhu, X. Li, W. C. H. Choy, *Nanoscale* **2016**, *8*, 3638.

[149] X. Chen, Z. Jia, Z. Chen, T. Jiang, L. Bai, F. Tao, J. Chen, X. Chen, T. Liu, X. Xu, C. Yang, W. Shen, W. E. I. Sha, H. Zhu, Y. (Michael) Yang, *Joule* **2020**, *4*, 1594.

[150] Q. Zeng, L. Liu, Z. Xiao, F. Liu, Y. Hua, Y. Yuan, L. Ding, *Sci. Bull.* **2019**, *64*, 885.

[151] K. Lang, Q. Guo, Z. He, Y. Bai, J. Yao, M. Wakeel, M. S. Alhodaly, T. Hayat, Z. Tan, *J. Phys. Chem. Lett.* **2020**, *11*, 9596.

[152] C. J. Traverse, R. Pandey, M. C. Barr, R. R. Lunt, *Nat. Energy* **2017**, *2*, 849.

[153] Q. Xue, R. Xia, C. J. Brabec, H.-L. Yip, *Energy Environ. Sci.* **2018**, *11*, 1688.

[154] C.-C. Chen, L. Dou, J. Gao, W.-H. Chang, G. Li, Y. Yang, *Energy Environ. Sci.* **2013**, *6*, 2714.

[155] L. Zuo, X. Shi, W. Fu, A. K.-Y. Jen, *Adv. Mater.* **2019**, *31*, 1901683.

Fateh Ullah obtained his M.Sc. and M.S. (organic chemistry) from Hazara University and COMSATS University (formerly known as COMSATS Institute of Information Technology), respectively. He obtained his Ph.D. from Zhejiang University, China, under the supervision of Professor Hongzheng Chen in 2017. After that, he worked as a postdoctoral researcher at the School of Materials Science and Engineering, Shanghai Jiao Tong University (SJTU). His research interests include synthesis, characterization, and application of organic conjugated materials for optoelectronic devices.

Chun-Chao Chen is an associate professor in the School of Materials Science and Engineering, Shanghai Jiao Tong University (SJTU). His research interests are organic semiconductor materials, devices, and physics for energy applications. He has demonstrated the first visibly transparent organic photovoltaic and triple-junction organic tandem solar cells.

Wallace C. H. Choy is a full professor in the Department of EEE, HKU. His research interests cover organic/inorganic optoelectronic devices, plasmonic structures, metal oxides, and nanomaterial devices.